Interfacial mass transfer limitations of the Fischer-Tropsch synthesis operated in a slurry bubble column reactor at industrial conditions

Camilla Berge Vik, Jannike Solsvik, Magne Hillestad, Hugo A. Jakobsen

Department of Chemical Engineering, Norwegian University of Science and Technology (NTNU), N-7491 Trondheim, Norway

Abstract

At high catalyst volume fractions the Fischer-Tropsch synthesis (FTS) operated in a slurry bubble column (SBC) is driven into the mass transfer limited regime. This study utilized literature models for the gas-liquid mass transfer coefficients in a multifluid-population balance model in which the gas-phase composition was a function of bubble size. The results confirmed that mass transfer limitations occur and that the choice of mass transfer coefficient model is crucial, yielding final conversion results ranging from 45% to 92% depending on the choice of k_L models. At smaller k_L values the composition is highly dependent on bubble size, whilst for the largest k_L values the composition is not a function of bubble size at all. The population balance modeling (PBM) allowed for explicitly keeping track of the bubble size distribution. Varying the inlet Sauter-mean diameter (SMD) resulted in a linear decrease in conversion as the inlet SMD was increased from 5 mm to 20 mm. Illustrative models for the bubble size dependency of k_L were implemented, which provided additional information compared to traditional models which use (bubble size) averaged values for the liquid-phase mass transfer coefficient k_L and/or the gas-liquid interfacial area

Email addresses: camilla.berge.vik@ntnu.no (Camilla Berge Vik), jannike.solsvik@ntnu.no (Jannike Solsvik), magne.hillestad@ntnu.no (Magne Hillestad), hugo.a.jakobsen@ntnu.no (Hugo A. Jakobsen)

a and composition.

Keywords: mass transfer coefficient, mass transfer, bubble size, Fischer-Tropsch, slurry bubble column, population balance equation

---

1. Introduction

Bubble column and slurry bubble column (SBC) reactors are widely used in the chemical, biochemical, petroleum and metallurgical industries (Leonard et al., 2015). Bubble column reactors and the mathematical models to describe them are presented in e.g. Deckwer (1992); Jakobsen (2014). Bubble column applications include different types of chemical reactions such as oxidation, chlorination, alkylation, polymerization, esterification and hydrogenation (Leonard et al., 2015). Bubble columns can also be used for fermentation, biological wastewater treatment and the production of liquid fuels from synthesis gas through the Fischer-Tropsch synthesis (FTS) (Leonard et al., 2015), an example of gas-to-liquid processes. A review of gas-to-liquid processes in slurry reactors is given in Wang et al. (2007). This study considers the FTS in an SBC, illustrated in Figure 1.

1.1. The FTS

The FTS is of interest when seeking renewable sources for liquid fuels. Lignocellulosic material such as forestry residue is a potential raw material for advanced biofuels. Torrefied and gasified biomasses are converted to hydrocarbons via synthesis gas. The FTS produces hydrocarbons of various lengths from synthesis gas over a catalyst through the reaction:

$$\mathrm{nCO} + (2\mathrm{n}+1)\mathrm{H_2} \rightarrow \mathrm{C_nH_{2n+2}} + \mathrm{nH_2O} \tag{1}$$

The catalyst type applied in this study is cobalt. Most biomass-to-liquid concepts have utilized cobalt, as it can be operated at higher conversion rates (Imhof and van der Waal, 2013). In this work a conventional 25 wt%$\mathrm{Co/Al_2O_3}$ catalyst is applied.

The kinetic model by Yates and Satterfield (1991) was applied in this study, given as:

$$-r_{CO} = \frac{a p_{CO} p_{H_2}}{(1 + b p_{CO})} \tag{2}$$

where p_{CO} and p_{H_2} are the partial pressures of CO and H_2 and a and b are temperature-dependent kinetic parameters. Eq. (2) was re-written into liquid concentrations by reformulating the partial pressures in terms of liquid concentrations by use of a Henry's law constant (as in e.g. Sehabiague et al. (2008); Troshko and Zdravistch (2009)) to obtain for Eq. (2):

$$-r_{CO} = \frac{a K_{H_2} x_{H_2} K_{CO} x_{CO} p^2}{(1 + b K_{H_2} x_{H_2} p)} \tag{3}$$

where p is pressure, K_s is the constant for species s and x_s is the liquid mole fraction of species s. Values for K_s were calculated by means of Aspen HYSYS.

A possible maximum catalyst concentration to be used in commercial practice was suggested around 40 vol% solids per volume of gas-free slurry (Maretto and Krishna, 1999). A high catalyst concentration is desired in order to maximize conversion of reactants into products. But it also drives the FTS into a mass transfer-controlled regime (Inga and Morsi, 1996). A catalyst concentration of 44 vol% solids per volume of gas-free slurry is applied in this study. The FTS is highly exothermic and efficient heat exchange is one of the reasons that the FTS is often operated in an SBC. Physical properties, reactor dimensions and operating conditions are given in Table 1. Additional relations are given in Appendix A.

1.2. Mass transfer resistances in the FTS

SBCs are gas-liquid-solid contactors. It is thus important to facilitate efficient transfer of mass and energy between the phases. A key element in the FTS is the transfer of reactants from inside the gas bubble, via the liquid phase and into the catalyst pores as illustrated in Figure 2. The resistances are (1) transport of reactants from bulk gas phase to gas-liquid interface, (2) transport of reactants from gas-liquid in-

terface to the bulk liquid, (3) transport of the reactants to the catalyst surface, (4) intra-particle diffusion of reactants into the pores of the catalyst, (5) adsorption of reactants on the active sites of the catalyst and (6) surface reaction of reactants to yield products (Kohler, 1986). The diffusion coefficient, which the mass transfer coefficient generally depends on, is much larger for gases than for liquids. Thus the gas-film resistance (1) is much smaller than the liquid-film resistance (2). With the reactor operating in the heterogeneous or churn-turbulent regime, the resistance of the transport through the liquid bulk phase can be considered small (Basha et al., 2015). Dorling et al. (1948) found that the catalytic activity for iron catalysts for the FTS was confined to a layer of 75 μm. This has been taken as evidence that for catalyst particles of size less than 150 μm, intra-particle diffusion resistance (4) is small (Satterfield and Huff, 1980). The liquid-side mass transfer coefficient is thus the dominating resistance to mass transfer in the FTS, as also concluded by other authors (Basha et al., 2015; Calderbank et al., 1963; Kohler, 1986; Satterfield and Huff, 1980), and the overall resistance from inside the gas bubble to converted products is mainly the sum of the mass transfer resistance and the kinetic resistance; (5)+(6). It is noted that also the liquid density and the solubility of the species to be transported are of relevance.

1.3. Mass transfer modeling

The mass transfer of species s across a liquid film is commonly modeled as a product of the interfacial area, the mass transfer coefficient and the driving force across the liquid film:

$$\Gamma_s = a_L k_{L,s} \rho_L (\omega^*_{L,s} - \omega_{L,s}) \tag{4}$$

where a_L is the gas-liquid interfacial area, $k_{L,s}$ the liquid-phase mass transfer coefficient, ρ_L the liquid density and $\omega^*_{L,s}$,$\omega_{L,s}$ the weight fractions of species s at the interface and in the bulk liquid, respectively. a_L and $k_{L,s}$ or their product $k_{L,s}a_L$ are generally system dependent and must be parameterized with the use of experimental data relevant for the system studied. Many experimental studies are reported for (slurry) bubble columns, but very few for high pressures and temperatures (Basha

et al., 2015; Rollbusch et al., 2015). Furthermore, most studies are carried out with water as the liquid phase (Rollbusch et al., 2015). It follows that a_L and $k_{L,s}$ are notoriously difficult to determine for the FTS operated at industrial conditions – which are typically temperatures of 473–513 K for high molecular mass products (Dry, 2002) and pressures around 3 MPa.

One step on the way to tackle the challenge in determining the volumetric mass transfer coefficient $k_{L,s}a_L$ is to use a population balance approach. This model describes the evolution of a mass or number density of bubbles in the reactor. The interfacial area a_L can then be calculated from moments of the density function and the problem is reduced to finding an empirical expression for the mass transfer coefficient $k_{L,s}$. The PBE is described in the textbooks by e.g. Jakobsen (2014); Ramkrishna (2000); Randolph and Larson (1988). A recent review of its foundation is found in Solsvik and Jakobsen (2015).

Knowledge about the number or mass of bubbles as function of their size and location allows for an interfacial area as a function of bubble size. Further, as different bubble sizes have different residence times due to the size-dependent momentum transfer, in particular the drag force, it is natural to consider bubble size dependent weight fractions – and possibly also bubble size dependent temperatures. Combined with a PBE this enables detailing the species mass transfer term in Eq. (4) with a size-dependent concentration gradient. For a cross-sectionally averaged model this yields:

$$f_d(z,\xi)\gamma_s(z,\xi) = \frac{f_d(z,\xi)A(\xi)}{\rho_G(z,\xi)V(\xi)} k_{L,s}(z,\xi)\rho_L(\omega^*_{L,s}(z) - \omega_{L,s}(z)) \tag{5}$$

where $f_d(z,\xi)$ is the mass density of bubbles of diameter ξ at location z at time t, $\gamma_s(z,\xi)$ is the bubble size dependent mass transfer term for species s, $\rho_G(z,\xi)$ is the gas density, $A(\xi)$ is the bubble surface area, $V(\xi)$ is the bubble volume and the interfacial concentration is approximated as:

$$\omega^*_{L,s}(z) \approx \frac{1}{K_s}\omega_{G,s}(z,\xi) \tag{6}$$

where K_s is a gas-liquid equilibrium constant for species s.

1.4. Previous work

Numerous modeling studies have been reported for the FTS, a recent overview is provided by Basha et al. (2015). Two previous studies are found in the literature for multiphase-PBE models applied to the FTS. Troshko and Zdravistch (2009) combined a sectional PBE (i.e. with the density function divided into discrete size classes) with two-fluid Eulerian equations in ANSYS-Fluent at isothermal conditions. The liquid and solid phases were assumed to be perfectly mixed. A bubble size averaged velocity was applied in the dispersed phase momentum equation. Basha et al. (2016) modeled the FTS in an SBC in ANSYS-Fluent using an Eulerian multiphase approach. The PBE was applied to keep track of the change in bubble size due to coalescence and breakage through a density function. A bubble size averaged velocity was applied in the dispersed phase momentum equation. The species mass equations were not reported, but the total mass transfer term was modeled using a previously developed empirical expression for the volumetric liquid-phase mass transfer coefficient (k_La). Thus the impact of the bubble size distribution on the interfacial area and subsequently mass transfer was not fully taken into account. In both Basha et al. (2016) and (Troshko and Zdravistch, 2009) the turbulence was included with use of the k-ϵ model. Vik et al. (2015) applied a cross-sectionally averaged continuous multifluid-PBE model as derived by Dorao (2006); Nayak et al. (2011); Patruno (2010); Solsvik and Jakobsen (2014) to the FTS. This model extends the study by Vik et al. (2015) with the multifluid-PBE model derived in Vik et al. (2018) with bubble size dependent composition and temperature.

In order to study mass transfer, the resistance of mass transfer in comparison to other resistances must be significant. The relative importance of mass transfer versus kinetic limitations for the FTS has been a subject of dispute (Deckwer et al., 1981a,b; Quicker and Deckwer, 1981; Satterfield and Huff, 1980, 1981). Inga and Morsi (1996) studied the relative importance of mass transfer using computer simulations and found that at high solids loading the process is driven into a mass transfer-controlled

regime. The maximum reactor performance was found at 37-40 wt% solids in gas-free slurry. The review by Wang et al. (2007) addressed this discussion and pointed out that for high reactor productivity, high gas superficial velocities and high solids concentration are advantageous. However, mass transfer may become a rate-limiting step at these operating conditions. In a recent study, Sehabiague and Morsi (2013a) used computer simulations applying various kinetic expressions for iron and cobalt catalysts. The results were again that at high solids concentrations, the reactor operated is in a mass-transfer controlled regime.

Sehabiague and Morsi (2013b) measured the product k_La and bubble size distributions in actual Fischer-Tropsch cuts. Basha et al. (2015) reviewed correlations for k_La applicable to SBC. Most studies in the review by Basha et al. (2015) study k_La, called the volumetric liquid-phase mass transfer coefficient. Furthermore, in experimental investigations such as those reported by Sehabiague and Morsi (2013b) only the averaged k_La value for the entire bubble bed is reported.

1.5. The originality of this work

The aim of this study is to describe how, in mass transfer limited processes such as the FTS in an SBC, bubble composition varies depending on bubble size. Previous work was mostly focused on the column average value of the volumetric mass transfer coefficient k_La and a composition which was independent of bubble size.

In this work a local and bubble size dependent interfacial area a_L is calculated directly from the PBE and combined with a local value of k_L. In this way mass transfer as a function of bubble size and spatial location can be quantified. With the mass transfer term defined as in Eq. (5) a local mass transfer coefficient which depends explicitly on bubble size $k_L(z, \xi)$ can be utilized. Literature correlations for k_L for the FTS, including those which depend on bubble size, are combined with a range of values for the inlet Sauter-mean diameter (SMD) d_s to study the impact of bubble size on mass transfer limitations in the FTS operated in an SBC at industrial conditions.

2. Volumetric mass transfer theory

2.1. The gas-liquid mass transfer coefficient

Discussions of mass transfer theories can be found in e.g. Beenackers and Van Swaaij (1993); Han et al. (2011, 2016); Jakobsen (2014); Kulkarni (2007) and Nedeltchev (2017). Selected mass transfer theories are illustrated in Figure 3 and briefly summarized in the sequel. Early models include the stagnant *film models* by Nernst (1904) and Lewis and Whitman (1924), deriving k_L from Fick's law. Higbie (1935) and Danckwerts (1951) considered a renewal of the liquid side of the interface by introducing the *surface renewal theory* and the *slip penetration theory*, respectively. By coupling the mass transfer equation with the momentum equation and assuming idealized flow conditions an analytical solution for the mass transfer coefficient can be obtained through the Sherwood, Reynolds and Schmidt numbers. The *solid sphere model* by Frössling (1938) and the *laminar boundary layer analysis* are both examples of this approach and are similar in form, but represent different flow situations. Frössling (1938) describes flow around a sphere and the laminar boundary layer analysis describes laminar flow along a flat wall. The *eddy models* formulate k_L as a function of the turbulence in the liquid phase. Rzehak (2016) broadly classified mass transfer models into two types, based on whether i) laminar or (ii) turbulent mechanisms determined the mass transfer. Following the classification by Rzehak (2016) the *eddy models* as indicated in Figure 3 represent turbulent models and the rest would be laminar.

Table 2 summarizes factors which influence the value of k_L. For our work two issues are of particular importance; factors which govern the bubble size dependency of k_L and factors which indicate whether the correlation is applicable to FTS conditions (Table 1). These will be discussed in the sequel.

2.1.1. Factors relevant for bubble size

The factors which relate the liquid-phase mass transfer coefficient k_L to bubble size are the contact time, the internal circulation in the bubble, the relative velocity

between the bubble and the liquid, the level of contamination or surface agents, the surface mobility and the bubble shape. As the mass transfer correlations differ with respect to the factors they depend on (as highlighted in Rzehak (2016)), the discussion in the sequel applies only to the gas-liquid mass transfer correlation in which the factor discussed is actually included in the correlation.

The *contact time* is the time that a liquid element is in contact with the gas-liquid interface and thus the time that the liquid element is available to exchange mass with the gaseous phase, such as a bubble. Smaller bubbles tend to have a lower velocity than larger bubbles as smaller bubbles have less buoyancy forces relative to their drag forces. Smaller bubbles thus have a longer contact time. According to Higbie (1935) a longer contact time decreases k_L as the driving force across the gas-liquid interface decreases. With respect to contact time k_L thus decreases with decreasing bubble size.

The term *internal circulation* refers to the mixing process inside the bubble. Perfect mixing (as assumed in the study by Higbie (1935)) yields a higher value for k_L than the case with no mixing (as was assumed in the "solid sphere" model in the study by Frössling (1938)). In general, larger bubbles experience more deviations from spherical shape and thus more stretching and deformation which again encourages internal circulation. Larger bubbles thus have better internal circulation. With respect to internal circulation k_L thus decreases with decreasing bubble size.

In a *contaminated* system the interface properties between the dispersed and the continuous phases are altered due to surface agents or other substances. Contamination immobilizes a surface (Olsen et al., 2017) and thus decreases k_L as it reduces surface mobility and renewal, increasing the contact time. Smaller bubbles are more easily contaminated (Calderbank and Moo-Young, 1961) and thus their surface is more easily immobilized. With respect to contamination smaller k_L thus decreases with decreasing bubble size.

The influence of *bubble shape* on k_L was discussed in the studies by e.g. Nedeltchev (2017) and Olsen et al. (2017). The bubble shape strongly influences the drag force

on the bubble and thus on the relative velocity between the bubble and the liquid through the drag coefficient (e.g. Tomiyama (1998)). The relative velocity is a function of bubble size. For air-water systems the relative velocity increases sharply as the bubble size increases to about 2 mm, where the bubble shape transition from spherical to elliptical shape takes place. After 2 mm the relative velocity increases with a smaller but still positive slope, as increasing bubble size results in increasing buoyancy and thus higher bubble velocity. In the correlations where k_L depends on the drag coefficient, the shape of the drag coefficient profile influences k_L.

2.1.2. Factors relevant for the FTS

The characteristics of the FTS in an SBC (Table 1) which influence the value of k_L are outlined in the sequel. The composition of the FTS liquid phase and the addition of solids leads to an increased continuous phase viscosity, which in turn reduces k_L (Yang et al., 2001). Furthermore, the solid particles may stick to the gas-liquid bubble interface and thus reduce the available interfacial area for mass transfer (Beenackers and Van Swaaij, 1993) and affect the thickness of the liquid film surrounding the bubble (Beenackers and Van Swaaij, 1993). As the solids fraction is very high in this study, the impact of solids is discussed in Appendix B. In short, the net effect of high solids fractions is likely to be reduced breakage and increased coalescence due to different mechanisms. The consequences for the terminal velocity involves knowledge on the surface chemistry of the solid, liquid and gaseous phases.

Studies involving mass transfer at elevated pressure were summarized by Rollbusch et al. (2015). They reported that some studies, such as that of Han and Al-Dahhan (2007) showed a slight negative effect of pressure on k_L, whilst other studies showed little effect. Fukuma et al. (1987) found that k_L is almost independent of pressure. The influence of temperature on k_L can be taken into account through the diffusion coefficient; either relying on the film theory ($k_L \propto D_L$) or the penetration theory ($k_L \propto D_L^{1/2}$). Hughmark (1967a) found that k_L was smaller for bubble swarms than for single bubbles. Calderbank and Moo-Young (1961) found that k_L decreased with

dispersion height due to higher residence time and thus more time for the system to become contaminated. Han et al. (2011) reported increasing k_L with increasing turbulent dissipation rate ϵ.

A suggestion for the most important factors to look for when searching the literature for a mass transfer correlation for the FTS at industrial conditions is thus temperature, superficial gas velocity / gas flow rate, level of liquid turbulence (connected to column diameter), addition of solids and liquid properties.

2.2. Gas-liquid mass transfer correlations

As no general mass transfer correlation can be found for the design of SBCs (Nedeltchev, 2017) one is left to survey the correlations available and select the most appropriate according to the parameters for the process. For complex systems which deviate from air-water systems at ambient conditions, it is common to develop correlations instead of using theoretical models for the liquid-phase mass transfer coefficient. The correlations rely on experimental results and are in general only applicable for the particular system they were designed for.

In this study twelve mass transfer correlations were found in the literature with application to the FTS, some also with dependency on bubble size in focus. These are given in Table 3. The mass transfer correlations were organized into four groups. The correlations in the first group of five correlations (Higbie (1935), Frössling (1938), Hughmark (1967a), Hughmark (1967b) and Brauer (1981)) depend on the single bubble size explicitly and were categorized as termed single bubble correlations. The members of the second group (Akita and Yoshida (1974), Fukuma et al. (1987)) depends on the SMD of the entire bubble swarm and termed SMD correlations. The third group (Fortescue and Pearson (1967), Lamont and Scott (1970) and Han et al. (2011)) were termed turbulent models as they relate k_L to the level of turbulence of the liquid phase. The final group was simply denoted "other correlations" and comprises the widely used model by Calderbank and Moo-Young (1961) and the FTS-specific correlation by Yang et al. (2001). In addition, two experimental values (from Deckwer et al. (1980) and from Vandu and Krishna (2004)) for the

liquid-phase mass transfer coefficient for CO in FTS liquids were included. The resulting k_L values for the conditions in Table 1 are shown in Figure 4. All correlations are shown in the same plot – with bubble size on the horizontal axis – to compare their magnitudes. The mass transfer correlations which do not explicitly depend on bubble size are thus shown as horizontal lines.

The single bubble size correlations all show a maximum value for bubble diameters slightly below 2 mm. For smaller diameters k_L decreases. For larger values of k_L the value either i) slightly decreases and then increases (in the correlations by (Brauer, 1981; Hughmark, 1967a)) or ii) decreases (in the correlations by (Frössling, 1938; Higbie, 1935)). The correlation by Frössling (1938) represents the smallest k_L value among the single bubble correlations. The correlation by Higbie (1935) represents the largest of the single bubble correlations. The correlations by Hughmark (1967a) and Brauer (1981) have similar shape as they are functions of the same variables, but with a different value for the fitting parameters. Including the models by Calderbank et al. (1963) in this discussion, the trend is a maximum k_L value at about 2 mm with a decrease in k_L for bubbles with a diameter of less than 2 mm. Thus when describing a system with many bubbles of size 2 mm and smaller, a bubble size dependent value for k_L can be necessary. For larger bubbles the single bubble size correlations are a weaker function of bubble size.

The SMD dependent correlations by Akita and Yoshida (1974) and Fukuma et al. (1987) both increase with increasing SMD. The slope is larger in the correlation by Fukuma et al. (1987) than in the correlation by Akita and Yoshida (1974). For bubble diameters of 5 mm the difference is a factor of two, but for bubble diameters of 12 mm the predictions are almost identical. Although the bubble size dependency in these correlations is given as an *average* bubble size for the entire bubble population, in contrast to the single bubble correlations discussed above, the correlations by Akita and Yoshida (1974) and Fukuma et al. (1987) suggest an opposite trend compared to the correlations proposed by Brauer (1981) and Hughmark (1967a).

The turbulent correlations (Fortescue and Pearson (1967), Lamont and Scott (1970) and Han et al. (2011)) do not depend explicitly on bubble size. An important

quantity in the turbulent models is the eddy size, which is discussed briefly in the sequel. A suitable review of the necessary turbulence theory is provided in Solsvik and Jakobsen (2016).

The key quantities in the turbulent mass transfer correlations are the smallest eddy length scale η (Kolmogorov scale) and the length scale of the energy containing eddies L (integral scale). The smallest length scale is defined in terms of the turbulence dissipation rate ϵ, which for bubble columns (in the absence of a more sophisticated quantification) can be approximated in terms of the inlet superficial velocity multiplied with the gravity acceleration. The length scale L, however, is not straightforward to determine. A natural approximation in the case of a bubble column with cooling rods, such as the FTS operated in an SBC, is to let L be the distance between the cooling rods. However, another possible approximation of the integral scale may be to set it equal to the hydraulic diameter of the column. The impact of the chosen approximation of the length scale L on the k_L value determined by the turbulent mass transfer coefficients by Fortescue and Pearson (1967); Han et al. (2011); Lamont and Scott (1970) is illustrated in Figure 5 as a function of turbulent dissipation rate. Circular markers indicate k_L values with channel width as the length scale L and no markers indicate k_L values with column hydraulic diameter as the length scale L. The correlations by Fortescue and Pearson (1967) and Han et al. (2011) show a reduction in k_L of close to a factor of 2 by choosing the hydraulic diameter instead of the channel width as the length scale L. This is a large discrepancy and should be given attention when using turbulent mass transfer correlations. The correlation by Lamont and Scott (1970) does not depend on L.

The length scale in the correlation by Yang et al. (2001) is neither the bubble size nor the eddy size, but in fact the column diameter to the power of -1. As the column diameter in their study was as low as 0.04 m the application of their correlation to a large column such as that in this case (Table 1) results in an unlikely low value for k_L. Their correlation is thus not considered further here.

2.3. Selection of liquid-phase mass transfer coefficient correlations for the FTS

The applicability of the correlations in Table 3 to the FTS in an SBC at the conditions described in Table 1 is addressed here. The correlation by Frössling (1938) was developed for droplets in air and is thus not applicable for bubbles in liquid, as is the case in FTS. The correlation by Yang et al. (2001) was developed in a too small column to be considered for industrial applications. The FTS conditions in Table 1 are outside the validity ranges specified for the correlations by Hughmark (1967a) and Fukuma et al. (1987). The FTS conditions are within the validity limits for the correlations by Higbie (1935), Akita and Yoshida (1974), Fortescue and Pearson (1967), Lamont and Scott (1970) and Brauer (1981) (please find dimensionless numbers in Appendix C.). This is a judgment made by the authors as the limits were not necessarily clearly stated, in particular in the study by Higbie (1935). The before-mentioned correlations were neither developed for paraffin-like liquids nor in the presence of solids which represents a weakness for application to the FTS. The correlation by Han et al. (2011) was validated for turbulent dissipation rates up to 0.5 m^2/s^3, but in our case the dissipation rate is estimated to be 2.55 m^2/s^3. With the widest selection of gases (including e.g. H_2) and liquids (including e.g. paraffin waxes) the correlation by Calderbank and Moo-Young (1961) appears most relevant among those in Table 3 as it takes the largest number of relevant factors into account.

It should be noted that none of the correlations in Table 3 are validated for all of the most important factors for the k_L for the FTS in the SBC at industrial conditions, as stated in Section 2.1.2. In the simulations in this study one representative mass transfer correlation from each group is employed. These are the correlations by: Higbie (1935) (single bubble diameter correlation), Akita and Yoshida (1974) (SMD correlation), Han et al. (2011) (turbulent correlation) and the "small" bubble correlation by Calderbank and Moo-Young (1961). In the article of Calderbank and Moo-Young (1961) are provided two correlations; one for "small" bubbles and one for "large" bubbles. The "small" bubble correlation is stated to be most appropriate for industrial flows with large dispersion heights and a significant amount of contam-

inants (Calderbank and Moo-Young, 1961) and is thus applied here. In addition, to cover the range of k_L values reported for the FTS in the literature, the experimental values of $k_L = 0.2$ mm/s (Deckwer et al., 1980) and $k_L = 3$ mm/s (Vandu and Krishna, 2004) are included.

2.4. Bubble sizes in the FTS

Authors have suggested widely different values for the SMD of the bubbles in the FTS operated in an SBC. Deckwer et al. (1980) reported a SMD of $d_s = 0.7$ mm for N_2 in paraffin with Al_2O_3 at pressures up to 1.1 MPa, a temperature of up to 543 K, catalyst weight fraction ϕ_S (wt% solids in gas-free slurry) up to 0.16 and u_G^s up to 0.04 m/s (homogeneous flow regime). Vandu and Krishna (2004) found that the main transport of reactants was performed by the "large" bubbles with diameters of as large as 20-70 mm. Their system was air in C_9-C_{11} at u_G^s up to 0.4 m/s (heterogeneous flow regime) with a catalyst weight fraction ϕ_S (wt% solids per wt gas free slurry) of up to 0.25. Sehabiague and Morsi (2013a) measured d_s in actual Fischer-Tropsch cuts and found d_s to vary between 3 mm and 20 mm. Pressure varied from 1–3 MPa, temperature up to 500 K, superficial gas velocity of 0.14-0.26 m/s and catalyst volume fraction ψ_S of 0-20 vol% solids per volume of gas-free slurry. Note that a volume fraction $\psi_S = 20$ vol% corresponds to about a weight fraction of $\phi_S = 5$-10 wt% (depending on the solid skeleton density) as the solid generally has a higher density than the liquid.

To investigate the effect of bubble size on mass transfer five different inlet SMD will be simulated in this work; $d_s = 5$ mm, $d_s = 8$ mm, $d_s = 10$ mm, $d_s = 15$ mm and $d_s = 20$ mm.

To illustrate the effect of a bubble size dependent k_L value, two models for k_L with the same mean but with different dependency on ξ are required. As no such pair of models were found in the literature it was constructed for illustrative purposes and shown in Figure 6.

3. Multifluid-PBE model

The multifluid-PBE model used in this work was described in a previous paper (Vik et al., 2018). In order to simulate the FTS in an SBC with liquid and solids phases along with the dispersed phase within a reasonable time frame, the combined multifluid-PBE model equations are simplified to 1D in space by cross-sectional averaging. The implemented equations for the dispersed phase are given below.

3.1. Implemented equations

The equation of change for total mass is given as:

$$\frac{\partial(f_d(z,\xi)v_z(z,\xi))}{\partial z} + \frac{\partial(f_d(z,\xi)v_\xi(z,\xi))}{\partial \xi} = f_d(z,\xi)\gamma(z,\xi) + S_m(z,\xi) \tag{7}$$

where $f_d\gamma$ is a mass transfer term and S_m is the source term due to coalescence and breakage. The boundary conditions are given as:

$$\begin{aligned} f_d|_{z=0} &= f_{d,\text{in}} \\ f_d|_{\xi=\xi_{\min}} &= 0 \end{aligned} \tag{8}$$

where $f_{d,\text{in}}$ is given as a normal distribution:

$$f_{d,\text{in}} = \frac{A}{\sigma\sqrt{2\pi}}\exp\left[(-(\xi-\overline{\xi})^2/(2\sigma^2))\right] \tag{9}$$

The growth flux $v_\xi f_d$ is set to zero at the ξ boundaries so that no bubbles enter or leave the domain through growth. The equation of change for species mass is given by:

$$\begin{aligned} &\frac{\partial[f_d(z,\xi)v_z(z,\xi)\omega_{G,s}(z,\xi)]}{\partial z} + \frac{\partial[f_d(z,\xi)v_\xi(z,\xi)\omega_{G,s}(z,\xi)]}{\partial \xi} \\ &= \frac{\partial}{\partial z}\left[f_d(z,\xi)D_{G,z,\text{eff}}\frac{\partial\omega_{G,s}(z,\xi)}{\partial z}\right] - f_d(z,\xi)\gamma_s(z,\xi) + S_{m\omega_s} \end{aligned} \tag{10}$$

where $f_d\gamma_s$ is the mass transfer term for species s. The boundary conditions are given as:

$$\begin{aligned} &\omega_{G,s}|_{z=0} = \omega_{G,s,\text{in}} \\ &\omega_{G,s}|_{\xi=\xi_{\min}} = K_s\omega_{L,s}(z) \\ &\frac{\partial\omega_{G,s}}{\partial z}|_{z=z_{\max}} = 0 \end{aligned} \tag{11}$$

The second boundary condition in Eq. (11) implies that the smallest bubbles with diameter $\xi_{\min}$ are assumed to be in gas-vapor equilibrium with the liquid phase at all times. Maretto and Krishna (1999) describe how bubbles of size 1-10 mm are entrained in the liquid phase. Entrained bubbles reach an equilibrium with the surrounding liquid relatively quickly as they travel along with the same segment of liquid most of the time. Although evidence suggests that bubbles of size 10 mm are too large to be trapped in the liquid phase, the chosen minimum bubble size limit of 0.1 mm is set well below the suggested value and thus believed to be reasonable. Eq. (10) was solved for all 12 species; CO, H_2, H_2O, CO_2, C_1, C_2, C_3, C_4, C_5-C_{12}, C_{13}-C_{22}, C_{23}-C_{30} and C_{31+}. The continuous (liquid phase) equation of change for species mass is given in Appendix A.2.

The dispersed phase equation of change for momentum is given by:

$$\begin{aligned} &f_d(z,\xi)v_z(z,\xi)\frac{\partial v_z(z,\xi)}{\partial z} + f_d(z,\xi)v_\xi(z,\xi)\frac{\partial v_z(z,\xi)}{\partial \xi} \\ &= \frac{\partial}{\partial z}\left[f_d(z,\xi)\frac{\mu_{G,z,\text{eff}}}{\rho_G(z,\xi)}\frac{\partial v_z(z,\xi)}{\partial z}\right] + f_d(z,\xi)F_{G,z}(z,\xi) + S_{mv_z} \end{aligned} \tag{12}$$

with the boundary conditions:

$$\begin{aligned} &v_z|_{z=0} = v_{G,\text{in}} \\ &v_z|_{\xi=\xi_{\min}} = v_L(z) \\ &\frac{\partial v_z}{\partial z}|_{z=z_{\max}} = 0 \end{aligned} \tag{13}$$

where the smallest bubbles are assumed to have the same velocity as the liquid. The equation of change for temperature is given by:

$$\begin{aligned} &f_d(z,\xi)C_p(z,\xi)v_z(z,\xi)\frac{\partial T_G(z,\xi)}{\partial z} + f_d(z,\xi)C_p(z,\xi)v_\xi(z,\xi)\frac{\partial T_G(z,\xi)}{\partial \xi} \\ &= \frac{\partial}{\partial z}\left[f_d(z,\xi)\frac{\lambda_{G,z,\text{eff}}}{\rho_G(z,\xi)}\frac{\partial T_G(z,\xi)}{\partial z}\right] + f_d(z,\xi)q_{G,z}(z,\xi) + S_{mh} \end{aligned} \tag{14}$$

where $f_d(z,\xi)q_{G,z}(z,\xi)$ is a heat transfer term. The boundary conditions are given as:

$$\begin{aligned} &T_G|_{z=0} = T_{G,\text{in}} \\ &T_G|_{\xi=\xi_{\min}} = T_{SL}(z) \\ &\frac{\partial T_G}{\partial z}|_{z=z_{\max}} = 0 \end{aligned} \tag{15}$$

where the smallest bubbles are assumed to have the same temperature as the slurry. Cross-sectionally averaged equations for the liquid and solid phases can be found e.g. in the textbook by Jakobsen (2014) and were applied to the FTS in an SBC in a previous publication (Vik et al., 2015). It is noted that one pseudo-homogeneous temperature equation is used for the slurry phase as the solid and liquid are assumed to have the same temperature. Furthermore, the species mass balance is not relevant for the solid phase as a uniform composition is assumed for the solid material of the catalyst particle.

The source terms due to coalescence and breakage in the dispersed phase equations of change for species mass, momentum and enthalpy were simplified to be linear functions of composition, velocity and enthalpy, respectively (Vik et al., 2018):

$$\langle S_{m\omega_s} \rangle \approx \omega_s S_m \tag{16}$$

$$\langle S_{mv_z} \rangle \approx v_z S_m \tag{17}$$

$$\langle S_{mh} \rangle \approx h S_m \tag{18}$$

The simplifications in the previous equations should be replaced by continuous source terms which redistribute the species mass, velocity and enthalpy between the bubble classes due to coalescence and breakage events. Buffo and Alopaeus (2017) proposed a source term on the discrete form for the species mass equation and Krepper et al. (2008) have implemented a source term for the distribution of momentum between the particle classes (but the explicit model was not given in the article). However, as the derivation of these source terms is not evident, it remains as further work to develop the continuous form of these terms and implement them into the current model.

3.2. Simulations

The dispersed phase equations (Eq.s (3)– (7)) combined with the equations for the liquid and solid phases and suitable closures were implemented in MATLAB®. The set of model equations was solved using orthogonal collocation. Table 4 lists the simulations performed.

4. Results and discussion

4.1. Effect of the gas-liquid mass transfer coefficient

The transfer correlations listed in Section 2.3 and their effect on conversion of reactant is shown in Figure 7. The inlet SMD was 10 mm for all simulations and the catalyst concentration was 44 vol% solid per gas free slurry. The left plot in Figure 7 shows k_L and the right plot shows conversion. The smallest k_L value of 0.2 mm/s results in 45 % final (at the reactor outlet) conversion. The highest k_L value results in a final conversion of 93%, which represents an increase by a factor of two compared to the lowest k_L values. The correlation by Calderbank and Moo-Young (1961) represents a conversion of almost 70%, that by Higbie (1935) a value of closer to 80% and finally the correlations by Akita and Yoshida (1974) and Han et al. (2011) yield a final conversion of 85% and 88%, respectively. With a range of 20 percentage points between the smallest and largest correlation value for k_L and a range

of 45 percentage points between the smallest and largest experimental value for k_L it appears evident that mass transfer limitations play a role for the FTS operated in an SBC at the simulated conditions. Thus an accurate k_L value is important.

4.2. Effect of inlet SMD

A decrease in inlet SMD increases the interfacial area a_L and, if the process is mass transfer limited, increases conversion. The inlet gas volume fraction and inlet gas superficial velocity were kept constant at $\alpha_G^0 = 0.5$ and $v_z^{s,0} = \alpha_G^0 v_z^0 = 0.26$ m/s. Figure 8 shows the conversion of CO for inlet d_s of 5, 8, 10, 15 and 20 mm. The conversion is 85% for an inlet SMD of 5 mm, decreasing steadily to just below 40% for an inlet SMD of 20 mm. The decrease in final conversion with increasing bubble diameter is approximately linear, as shown in Figure 9. Thus for the simulated conditions the bubble size is important for mass transfer efficiency.

4.3. Bubble size dependent composition

Conversion of CO as a function of both reactor location and bubble size for k_L values 0.2 mm/s, 0.4 mm/s and 3 mm/s are shown in Figure 10. For $k_L = 0.2$ mm/s the weight fraction of CO in the dispersed phase is a strong function of bubble size. The smallest bubble size is in equilibrium with the liquid phase at all times and thus close to zero as all the reactants are consumed close to the outlet. The smallest bubbles except the boundary condition have a weight fraction of reactant of 0.1 at the reactor outlet. The largest bubbles have a weight fraction of reactant of more than 0.5. Thus as also indicated in Figure 7, $k_L = 0.2$ mm/s results in a mass transfer limited system in which the bubble composition is a strong function of bubble size. For $k_L = 0.4$ mm/s the largest bubbles have slightly less reactant remaining – a weight fraction of 0.4. The bubble size dependency is strong also in this case, i.e. the k_L value predicted by Calderbank and Moo-Young (1961) yields a mass transfer limited system for the current process conditions. In contrast, $k_L = 3$ mm/s shows an approximately flat weight fraction profile of CO as a function of bubble size at the outlet of the reactor.

Thus with a k_L value of 3 mm/s there are no detectable mass transfer limitations in the system and the bubble size is unimportant with respect to conversion.

4.4. Bubble size dependency of the liquid-phase mass transfer coefficient

The dependency of k_L on bubble size was discussed in Section 2.1.1 and 2.2. The mass transfer $\gamma_s(z, \xi)$ is a function of both the axial location in the reactor and bubble size as shown for the reactant CO in Figures 11–13. Figure 11 compares the local mass transfer term for the mass transfer correlations by Calderbank and Moo-Young (1961) an Higbie (1935). As seen in Figure 4 the correlation by Higbie (1935) takes on a maximum value for bubble diameters around 2 mm whilst the correlation by Calderbank and Moo-Young (1961) is not a function of bubble size. This can be observed in Figure 11 as the mass transfer for the bubble sizes below 5 mm diameter is larger in the lower plot (Higbie) than in the upper plot (Calderbank and Moo-Young). The effect of the bubble size dependency of k_L on conversion is overshadowed by the fact that the k_L value by Higbie (1935) is higher than the value by Calderbank and Moo-Young (1961). Furthermore, the SMD is as large as 10 mm in the simulations which means that the number of bubbles of size around 2 mm is close to zero. Thus an effect of the bubble size dependency of k_L is better observed for systems with smaller bubble sizes.

Figure 12 compares the local mass transfer term for the k_L values predicted by Calderbank and Moo-Young (1961) with that of Akita and Yoshida (1974). Recalling Figure 4 the correlation by Akita and Yoshida (1974) predicts a larger k_L by a factor two to three for the relevant bubble size range. This can be seen in Figure 12 as a higher mass transfer flux closer to the inlet and a decrease in the mass transfer flux towards the outlet as most of the reactant is consumed. As k_L decreases when d_s decreases in the correlation by Akita and Yoshida (1974) the decrease in bubble size both due to bubble breakage and the reduction of number of moles of gas in the bubble contributes to a further decrease in mass transfer towards the outlet.

Finally, the mass transfer predictions with the two extreme k_L values from Deckwer et al. (1980) and Vandu and Krishna (2004) are compared in Figure 13. With the

high k_L value from Vandu and Krishna (2004) even the larger bubbles close to 15 mm are characterized with high mass transfer rates close to the inlet of the reactor. The high mass transfer rates for CO decrease significantly towards the outlet, as most of the reactant is consumed. The mass transfer with the low value for k_L from Deckwer (1980) results in a rather flat profile in the axial direction, as the mass transfer rate is so low that the amount of remaining reactant keeps large throughout the reactor. The mass transfer rate is larger for the smaller bubbles than the large ones due to their higher interfacial area per volume.

It was seen from Figure 4 that k_L, when it does depend on bubble size, has a maximum at bubble diameters of about 2 mm and rapidly decreases below 2 mm. Furthermore, Figure 9 showed that the conversion increased from about 40% for inlet SMD of 20 mm to almost 90% for inlet SMD of 5 mm. This indicates that mass transfer limitations are becoming much less important for bubble sizes below 2 mm. Thus the bubble size dependency of k_L, which is most prominent around and below 2 mm, is not likely to be important at the current operating conditions. However, for processes with large mass transfer limitations also at 2 mm bubble sizes, the bubble size dependency of k_L may become important.

k_L as a function of bubble size may also become important if the size dependency of k_L is more prominent at larger bubble sizes. For illustration purposes two constructed models for k_L with equal mean and opposite slopes (Figure 6) were applied in the study. The effect on composition and subsequently conversion is shown in Figures 14 and 15. The interfacial area and mean k_L were identical in the two cases. Figure 14 shows that the composition in the bubbles larger than approximately 8 mm are affected by the size dependency of k_L. Compared to model 1, model 2, with an increasing slope as a function of bubble size, shows less remaining reactant. Model 3, with a decreasing slope in k_L as a function of bubble size, results in more remaining reactant in the larger bubbles. The consequence on conversion is shown in Figure 15. Figure 15 shows that the model with increasing slope yields higher conversion than the model with decreasing slope. This result is due to that more bubbles of size above 7.5 mm diameter are present than bubbles of size less than 7.5 mm. Nevertheless,

the results show that the bubble size distribution, not only the interfacial area, affects conversion - as the interfacial area and k_L, and thus k_La was equal in the two illustrative cases. In other words, the multifluid-PBE model applied in this study provides more information than the models using an average value for k_L or a or even k_La.

5. Conclusion

The results with $k_L = 0.4$ mm/s (Calderbank and Moo-Young, 1961) show that the FTS is mass transfer limited at the simulated conditions. The impact of bubble size on conversion is thus important and the conversion increases linearly with decreasing inlet SMD – from about 40% for $d_s = 20$ mm to almost 90% for $d_s = 5$ mm.

A review of correlations for k_L for the FTS in an SBC was performed and none of the literature correlations take all of the desired conditions for the FTS at industrial conditions (temperature, superficial gas velocity, addition of solids, large column diameter and liquid properties) into account. Among the correlations found, the correlation by Calderbank and Moo-Young (1961) took most of the factors into account.

As the process is mass transfer limited at the current conditions, the choice of mass transfer correlation is crucial. Conversion ranges from 45% to 92% for d_s =10 mm depending on the choice of k_L value. Composition was a strong function of bubble size in the case of the smaller k_L values, as expected. For the high k_L values the composition was not a function of bubble size, but for the smaller values the difference in composition for the smallest and largest bubbles was significant. The larger bubbles were in a mass transfer limited regime, whilst the smaller were not. The multifluid-PBE model with size dependent composition provides insight into the importance of modeling the bubble size distribution.

The dependency of bubble diameter on k_L for the single bubble and the SMD correlations show opposite trends as a function of bubble size. This deserves further attention. The bubble size dependency was not fully utilized in this study as mass transfer

limitations diminished for inlet SMD below 5 mm. But for strongly mass transfer limited processes the multifluid-PBE model with bubble size dependent weight fractions can give valuable information.

The multifluid-PBE model applied in this study predicted different results for the two models for k_L which would in traditional models (with k_L not being a function of bubble size) give identical results. In this illustrative case increasing slope yielded higher conversion than decreasing slope. The results show that the bubble size distribution, not only the interfacial area, has an impact on the conversion, as the interfacial area and mean k_L were identical in the two cases but yielded different conversion.

As the value of k_L was found to be important and the bubble size dependency of k_L, indicated in the literature k_L models, was partly contradictory, a natural suggestion for further work is to improve the local and bubble size dependent model for k_L and its ability to capture the underlying physics.

6. Acknowledgments

M.Sc. Ida Kristine Kure is acknowledged for contributing in identifying and implementing some of the mass transfer correlations. The work was supported by the NTNU Department of Chemical Engineering (C. B. Vik) and the Research Council of Norway (J. Solsvik).

7. References

K. Akita and F. Yoshida. Bubble size, interfacial area, and liquid-phase mass transfer coefficient in bubble columns. *Industrial & Engineering Chemistry Process Design and Development*, 13(1):84–91, 1974.

S. Ata. Coalescence of bubbles covered by particles. *Langmuir*, 24(12):6085–6091, 2008.

O. M. Basha, L. Sehabiague, A. Abdel-Wahab, and B. I. Morsi. Fischer-Tropsch synthesis in slurry bubble column reactors: Experimental investigations and modeling – A review. *International Journal of Chemical Reactor Engineering*, 13(3): 201–288, 2015.

O. M. Basha, L. Weng, Z. Men, and B. I. Morsi. CFD modeling with experimental validation of the internal hydrodynamics in a pilot-scale slurry bubble column reactor. *International Journal of Chemical Reactor Engineering*, 14(2):599–619, 2016.

A. A. C. M. Beenackers and W. P. M. Van Swaaij. Mass transfer in gas-liquid slurry reactors. *Chemical Engineering Science*, 48(18):3109–3139, 1993.

H. Brauer. Particle fluid transport processes. *Progress in Chemical Engineering*, 19: 81–111, 1981.

A. Buffo and V. Alopaeus. A novel simplified multivariate PBE solution method for mass transfer problems. *Chemical Engineering Science*, 172:463–475, 2017.

P. H. Calderbank and M. B. Moo-Young. The continous phase heat and mass-transfer properties of dispersions. *Chemical Engineering Science*, 16:39–54, 1961.

P. H. Calderbank, F. Evans, R. Farley, G. Jepson, and A. Poll. Rate processes in the catalyst–slurry Fischer–Tropsch reaction. In J. M. Pirie, editor, *Proceedings of the Symposium on Catalysis in Practice, 20–21 June*. Institution of Chemical Engineers, London, 1963.

Y.-M. Chen and L.-S. Fan. Bubble breakage mechanisms due to collision with a particle in a liquid medium. *Chemical Engineering Science*, 44(1):117–132, 1989.

V. P. Chilekar, J. van der Schaaf, B. F. M. Kuster, J. T. Tinge, and J. C. Schouten. Influence of elevated pressure and particle lyophobicity on hydrodynamics and gas-liquid mass transfer in slurry bubble columns. *AIChE Journal*, 56(3):584–596, 2010.

P. V. Danckwerts. Significance of liquid-film coefficients in gas absorption. *Industrial and engineering chemistry*, 43(6):1460–1467, 1951.

J. de Swart, R. van Vliet, and R. Krishna. Size, structure and dynamics of 'large' bubbles in a two-dimensional slurry bubble column. *Chemical Engineering Science*, 51(20):4619–4629, 1996.

W.-D. Deckwer. On the mechanism of heat transfer in bubble column reactors. *Chemical Engineering Science*, 35(6):1341–1346, 1980.

W.-D. Deckwer. *Bubble Column Reactors*. Wiley, Surrey, 1992.

W.-D. Deckwer, R. Burckhart, and G. Zoll. Mixing and mass transfer in tall bubble columns. *Chemical Engineering Science*, 29(11):2177–2188, 1974.

W.-D. Deckwer, Y. Louisi, A. Zaidi, and M. Ralek. Hydrodynamic properties of the Fischer-Tropsch slurry process. *Industrial and Engineering Chemistry Process Design and Development*, 19(4):699–708, 1980.

W.-D. Deckwer, Y. Serpemen, M. Ralek, and B. Schmidt. On the relevance of mass transfer limitations in the Fischer-Tropsch slurry process. *Chemical Engineering Science*, 36(4):765–771, 1981a.

W.-D. Deckwer, Y. Serpemen, M. Ralek, and B. Schmidt. Response to letter of Satterfield and Huff concerning mass transfer limitations in the Fischer-Tropsch slurry reactors. *Chemical Engineering Science*, 36(4):791–792, 1981b.

C. A. Dorao. *High Order Methods for the Solution of the Population Balance Equation with Applications to Bubbly Flows*. PhD thesis, Norwegian University of Science and Technology, 2006.

T. A. Dorling, D. Gall, and C. C. Hall. Some factors affecting the activity of sintered iron catalysts for the Fischer-Tropsch synthesis. *Journal of Applied Chemistry*, 8 (9):533–549, 1948.

M. E. Dry. The Fischer-Tropsch process: 1950-2000. *Catalysis Today*, 71:227–241, 2002.

C. Erkey, J. B. Rodden, and A. Akgerman. Diffusivities of synthesis gas and n-alkanes in Fischer-Tropsch wax. *Energy & Fuels*, 4:275–276, 1990.

G. M. Evans, E. Doroodchi, G. L. Lane, P. T. L. Koh, and M. P. Schwarz. Mixing and gas dispersion in mineral flotation cells. *Chemical Engineering Research and Design*, 86(12):1350–1362, 2008.

G. Fortescue and J. Pearson. On gas absorption into a turbulent liquid. *Chemical Engineering Science*, 22:1163–1176, 1967.

N. Frössling. Über die verdunstung fallender tropfen. *Gerlands Beitraege zur Geophysik*, 52:170–216, 1938.

M. Fukuma, K. Muroyama, and A. Yasunishi. Specific gas-liquid interfacial area and liquid-phase mass transfer coefficient in a slurry bubble column. *Journal of Chemical Engineering of Japan*, 20(3):321–324, 1987.

J. Grienberger. *Untersuchung und Modellierung von Blasensäulen*. PhD thesis, Universität Erlangen-Nürnberg, 1992.

L. Han and M. Al-Dahhan. Gas-liquid mass transfer in a high pressure bubble column reactor with different sparger designs. *Chemical Engineering Science*, 62 (1–2):131–139, 2007.

667 L. Han, H. Luo, Y. Liu, K. You, and P. Liu. A multi-scale theoretical model for gas-
668 liquid interface mass transfer based on the wide spectrum eddy contact concept.
669 *AIChE Journal*, 57(4):886–896, 2011.

670 L. Han, J. Fu, M. Li, S. Gong, N. Gao, C. Zhang, and H. Luo. A theoretical unsteady-
671 state model for kl of bubbles based on the framework of wide energy spectrum.
672 *AIChE Journal*, 62(4):1007–1022, 2016.

673 R. Higbie. The rate of absorption of a pure gas into a still liquid during short periods
674 of exposure. *Transactions of the American Institute of Chemical Engineers*, 31:
675 365–389, 1935.

676 G. A. Hughmark. Holdup and mass transfer in bubble columns. *Industrial and*
677 *Engineering Chemistry Process Design and Development*, 6(2):218–220, 1967a.

678 G. A. Hughmark. Mass and heat transfer from rigid spheres. *AIChE Journal*, 13(6):
679 1219–1221, 1967b.

680 P. Imhof and J. C. van der Waal. *Catalytic Process Development for Renewable*
681 *Materials*. Wiley, Singapore, 2013.

682 J. R. Inga and B. I. Morsi. A novel approach for the assessment of the rate-limiting
683 step in Fischer-Tropsch slurry process. *Energy & Fuels*, 10(3):566–572, 1996.

684 H. A. Jakobsen. *Chemical Reactor Modeling: Multiphase Reactive Flows*. Springer,
685 Berlin, second edition, 2014.

686 M. A. Kohler. Comparison of mechanically agitated and bubble column slurry reac-
687 tors. *Applied Catalysis*, 22(1):21–53, 1986.

688 E. Krepper, D. Lucas, T. Frank, H.-M. Prasser, and P. J. Zwart. The inhomogeneous
689 MUSIG model for the simulation of polydispersed flows. *Nuclear Engineering and*
690 *Design*, 238(7):1690–1702, 2008.

691 A. A. Kulkarni. Mass transfer in bubble column reactors: Effect of bubble size
692 distribution. *Industrial & Engineering Chemistry Research*, 46(7):2205–2211, 2007.

693 J. C. Lamont and D. S. Scott. An eddy cell model of mass transfer on into the surface
694 of a turbulent liquid. *AIChE Journal*, 16(4):513–519, 1970.

695 C. Leonard, J.-H. Ferrasse, O. Boutin, S. Lefevre, and A. Viand. Bubble column
696 reactors for high pressures and high temperatures operation. *Chemical Engineering*
697 *Research and Design*, 100:391–421, 2015.

698 W. K. Lewis and W. G. Whitman. Principles of gas absorption. *Industrial and*
699 *engineering chemistry*, 16(12):1215–1220, 1924.

700 C. Maretto and R. Krishna. Modelling of a bubble column slurry reactor for Fischer-
701 Tropsch synthesis. *Catalysis Today*, 52(2-3):279–289, 1999.

702 C. Maretto and R. Krishna. Design and optimisation of a multi-stage bubble column
703 slurry reactor for fisher-tropsch synthesis. *Catalysis Today*, 66(2–4):241–248, 2001.

704 A. Nayak, Z. Borka, L. Patruno, F. Sporleder, C. Dorao, and H. A. Jakobsen. A
705 combined multifluid-population balance model for vertical gas-liquid bubble-driven
706 flows considering bubble column operating conditions. *Industrial & Engineering*
707 *Chemistry Research*, 50(3):1786–1798, 2011.

708 S. Nedeltchev. Theoretical prediction of mass transfer coefficients in both gas-liquid
709 and slurry bubble columns. *Chemical Engineering Science*, 157:169–181, 2017.

710 W. Nernst. Theorie der reaktionsgeschwindigkeit in heterogenen systemen.
711 *Zeitschrift für Physicalische Chemie*, 47(1):52–55, 1904.

712 S. Ojima, K. Hayashi, and A. Tomiyama. Effects of hydrophilic particles on bubbly
713 flow in a slurry bubble column. *International Journal of Multiphase Flow*, 58:
714 154–167, 2014.

715 S. Ojima, S. Sasaki, K. Hayashi, and A. Tomiyama. Effects of particle diameter on
716 bubble coalescence in slurry bubble column. *Journal of Chemical Engineering of*
717 *Japan*, 48(3):181–189, 2015.

718 J. E. Olsen, D. Dunnebier, E. Davies, P. Skjetne, and J. Morud. Mass transfer
719 between bubbles and seawater. *Chemical Engineering Science*, 161:308–315, 2017.

720 L. E. Patruno. *Experimental and Numerical Investigations of Liquid Fragmenta-*
721 *tion and Droplet Generation for Gas Processing at High Pressures*. PhD thesis,
722 Norwegian University of Science and Technology, 2010.

723 M. F. M. Post, A. C. Van't Hoog, J. K. Minderhoud, and S. T. Sie. Diffusion
724 limitations in Fischer-Tropsch catalysts. *AIChE Journal*, 35(7):1107–1114, 1989.

725 M. J. Prince and H. W. Blanch. Bubble coalescence and break-up in air-sparged
726 bubble columns. *AIChE Journal*, 36(10):1485–1499, 1990.

727 G. Quicker and W.-D. Deckwer. A further note on mass transfer limitations in the
728 Fischer-Tropsch synthesis. *Chemical Engineering Science*, 36(6):1577–1579, 1981.

729 D. Ramkrishna. *Population Balances: Theory and Applications to Particulate Sys-*
730 *tems in Engineering*. Academic Press, San Diego, 2000.

731 A. D. Randolph and M. A. Larson. *Theory of Particulate Processes*. Academic Press,
732 San Diego, second edition, 1988.

733 P. Rollbusch, M. Bothe, M. Becker, M. Ludwig, M. Grünewald, M. Schlüter, and
734 R. Franke. Bubble columns operated under industrial relevant conditions – current
735 understanding of design parameters. *Chemical Engineering Science*, 126:660–678,
736 2015.

737 R. Rzehak. Modeling of mass-transfer in bubbly flows encompassing different mech-
738 anisms. *Chemical Engineering Science*, 151:139–143, 2016.

739 A. R. Sarhan, J. Naser, and G. Brooks. CFD simulation on influence of suspended
740 solid particles on bubbles' coalescence rate in flotation cell. *International Journal*
741 *of Mineral Processing*, 146:54–64, 2016.

A. R. Sarhan, J. Naser, and G. Brooks. Effects of particle size and concentration on bubble coalescence and froth formation in a slurry bubble column. *Particuology*, 36:82–95, 2018.

C. N. Satterfield and G. A. Huff. Effects of mass transfer on Fischer-Tropsch synthesis in slurry reactors. *Chemical Engineering Science*, 35:195–202, 1980.

C. N. Satterfield and G. A. Huff. Mass transfer limitations in Fischer-Tropsch slurry reactors. *Chemical Engineering Science*, 36:791–792, 1981.

L. Sehabiague. *Modeling, Scaleup and optimisation of slurry bubble column reactors for Fischer-Tropsch synthesis*. PhD thesis, University of Pittsburgh, 2012.

L. Sehabiague and B. I. Morsi. Modeling and simulation of a Fischer-Tropsch slurry bubble column reactor using different kinetic rate expressions for iron and cobalt catalysts. *International Journal of Chemical Reactor Engineering*, 11(1):309–330, 2013a.

L. Sehabiague and B. I. Morsi. Hydrodynamic and mass transfer characteristics in a large-scale slurry bubble column reactor for gas mixtures in actual Fischer-Tropsch cuts. *International Journal of Chemical Reactor Engineering*, 11(1):83–102, 2013b.

L. Sehabiague, R. Lemoine, A. Behkish, Y. J. Heintz, M. Sanoja, R. Oukaci, and B. I. Morsi. Modeling and optimization of a large-scale slurry bubble column reactor for producing 10,000 bbl/day of Fischer-Tropsch liquid hydrocarbons. *Journal of the Chinese Institute of Chemical Engineers*, 39(2):169–179, 2008.

A. Shaikh and M. Al-Dahhan. Scale-up of bubble column reactors: A review of current state-of-the-art. *Industrial & Engineering Chemistry Research*, 52(24): 8091–8108, 2013.

J. Solsvik and H. A. Jakobsen. A combined multifluid-population balance model applied to dispersed gas-liquid flows. *Journal of Dispersion Science and Technology*, 35(11):1611–1625, 2014.

J. Solsvik and H. A. Jakobsen. The foundation of the population balance equation: A review. *Journal of Dispersion Science and Technology*, 36(4):510–520, 2015.

J. Solsvik and H. A. Jakobsen. A review of the statistical turbulence theory required extending the population balance closure models to the entire spectrum of turbulence. *AIChE Journal*, 62(5):1795–1820, 2016.

A. Tomiyama. Struggle with computational bubble dynamics. *Multiphase Science and Technology*, 10(4):369–405, 1998.

A. A. Troshko and F. Zdravistch. CFD modeling of slurry bubble column reactors for Fisher-Tropsch synthesis. *Chemical Engineering Science*, 64(5):892–903, 2009.

P. Tyagi and V. V. Buwa. Dense gas-liquid-solid flow in a slurry bubble column: Measurements of dynamic characteristics, gas volume fraction and bubble size distribution. *Chemical Engineering Science*, 173:346–362, 2017.

C. Vandu and R. Krishna. Volumetric mass transfer coefficients in slurry bubble columns operating in the churn-turbulent flow regime. *Chemical Engineering and Processing*, 43:987–995, 2004.

C. B. Vik, J. Solsvik, M. Hillestad, and H. A. Jakobsen. Modeling of a slurry bubble column reactor for the production of biofuels via the Fischer-Tropsch synthesis. *Chemical Engineering & Technology*, 38(4):690–700, 2015.

C. B. Vik, J. Solsvik, M. Hillestad, and H. A. Jakobsen. A multifluid–PBE model for simulation of mass transfer limited processes operated in bubble columns. *Computers & Chemical Engineering*, 110:115–139, 2018.

T. Wang, J. Wang, and Y. Jin. Slurry reactors for gas-to-liquid processes: A review. *Industrial & Engineering Chemistry Research*, 46(18):5824–5847, 2007.

Y. Xing, X. Gui, L. Pan, B.-E. Pinchasik, Y. Cao, J. Liu, M. Kappl, and H.-J. Butt. Recent experimental advances for understanding bubble-particle attachment in flotation. *Advances in Colloid and Interface Science*, 246:105–132, 2017.

G. Yang and L. Fan. Axial liquid mixing in high-pressure bubble columns. *AIChE Journal*, 49(8):1995–2008, 2003.

W. Yang, J. Wang, and Y. Jin. Mass transfer characteristics of syngas components in slurry system at industrial conditions. *Chemical Engineering & Technology*, 24 (6):651–657, 2001.

I. C. Yates and C. N. Satterfield. Intrinsic kinetics of the Fischer-Tropsch synthesis on a cobalt catalyst. *Energy & Fuels*, 5(1):168–173, 1991.

Nomenclature

Latin letters

A	[m^2]	bubble surface area
A	[kg m^{-1} m^{-3}]	amplitude of $f_{d,\text{in}}$, $A = \sum_\xi \frac{\alpha_{G,in}(\xi)\rho_{G,in}(\xi)\sigma\sqrt{(2\pi)}}{exp[-(\xi-\bar{\xi})^2/(2\sigma^2)]W_\xi(\xi)}$
a	[kmole s^{-1}(kg cat)$^{-1}$Pa^{-2}]	kinetic parameter
a_L	[m^2 m^{-3}]	interface area for gas-liquid interface
b	[Pa^{-1}]	kinetic parameter
C_p	[J K^{-1} kg^{-1}]	heat capacity
D_s	[m^{2}s^{-1}]	diffusion coefficient for species s
D_C	[m]	reactor inner diameter
$D_{G,z,\text{eff}}$	[m^2 s^{-1}]	effective axial dispersion coefficient
D_H	[m]	reactor hydraulic diameter
D_t	[m]	distance between cooling tubes
d_s	[m]	Sauter-mean diameter
d_S	[m]	solids average particle diameter
f_d	[kg m^{-1} m^{-3}]	mass density function
$F_{G,z}$	[kg m s^{-2}]	cross-sectionally averaged force term
g	[m s^{-1}]	standard acceleration due to gravity
h	[J kg^{-1}]	mass averaged enthalpy
H	[m]	reactor height
n	[mol]	number of moles
k	[m^{2}s^{-2}]	turbulent kinetic energy
K_s	[-]	weight based vapor-liquid equilibrium constant
k_L	[m s^{-1}]	liquid-phase mass transfer coefficient
p	[Pa]	pressure
$q_{G,z}$	[J kg^{-1}s^{-1}]	cross-sectially averaged heat transfer term

Q	[m^3 s^{-1}]	total flowrate
r_{CO}	[kmole s^{-1}(kg cat)$^{-1}$]	reaction rate of CO
S_m	[kg $m^{-1}m^{-3}$ s^{-1}]	source term due to coalescence and breakage in the equation of change for mass
$S_m\omega_s$	[kg $m^{-1}m^{-3}$ s^{-1}]	source term due to coalescence and breakage in the equation of change for species mass
$S_m v_z$	[kg m^{-3} s^{-2}]	source term due to coalescence and breakage in the equation of change for momentum
$S_m h$	[J m^{-3} m^{-1}]	source term due to coalescence and breakage in the equation of change for momentum
t	[s]	time
T	[K]	temperature
V	[m^3]	volume of bubble
v_L	[m s^{-1}]	cross-sectionally averaged liquid velocity
v_z	[m s^{-1}]	cross-sectionally averaged gas velocity
v_ξ	[m s^{-1}]	growth velocity
v_t	[m s^{-1}]	terminal velocity
w	[m]	wetted perimeter
x_s	[–]	mole fraction of s in the liquid phase
z	[m]	axial direction

803 *Greek letters*

α	[-]	volume fraction
γ	[s^{-1}]	size-dependent mass transfer term
γ_s	[s^{-1}]	size-dependent mass transfer term for species s

Γ_s	[kg m^{-3} s^{-1}]	mass transfer term for species s
ϵ	[m^{2}s^3]	volume fraction
η	[-]	Kolmogorov scale
$\lambda_{G,z,\text{eff}}$	[W m^{-1} K^{-1}]	effective turbulent conductivity in spatial space
μ	[Pa s]	viscosity
$\mu_{G,z,\text{eff}}$	[kg m^{-1}s^{-1}]	cross-sectionally averged effective (and turbulent) viscosity for the gas phase
ν	[m^2 s]	kinematic viscosity
ξ	[m]	bubble diameter
σ	[-]	standard deviation for the inlet distribution of $f_{d,\text{in}}$. $\sigma = 10 \times 10^{-4}$
σ_{G-L}	[N m^{-1}]	gas-liquid surface tension
ϕ_S	[-]	weight fraction solids in gas-free slurry
ψ_S	[-]	volume fraction solids in gas-free slurry
ρ	[kg m^{-3}]	density
$\omega_{G,s}$	[-]	mass fraction of species s in the gas phase
$\omega_{L,s}$	[-]	mass fraction of species s in the liquid phase

804 *Subscripts*

$_b$	bubble
$_c$	continuous
$_d$	dispersed
$_{\text{eff}}$	effective
$_G$	gas phase
$_{G-L}$	gas-liquid
$_{\text{in}}$	inlet
$_L$	liquid phase

$_L$	integral scale
$_{\max}$	maximum
$_{\min}$	minimum
$_s$	species s
$_S$	solid phase
$_{SL}$	slurry phase
$_t$	terminal
$_z$	axial (z) direction
$_\lambda$	Taylor scale

Superscripts

*	at the interface
^{0}	at the inlet
^{s}	superficial

Abbreviations

BC	bubble column
FTS	Fischer-Tropsch synthesis
ID	inner diameter
PBE	population balance equation
PBM	population balance model
SBC	slurry bubble column
SMD	Sauter-mean diameter

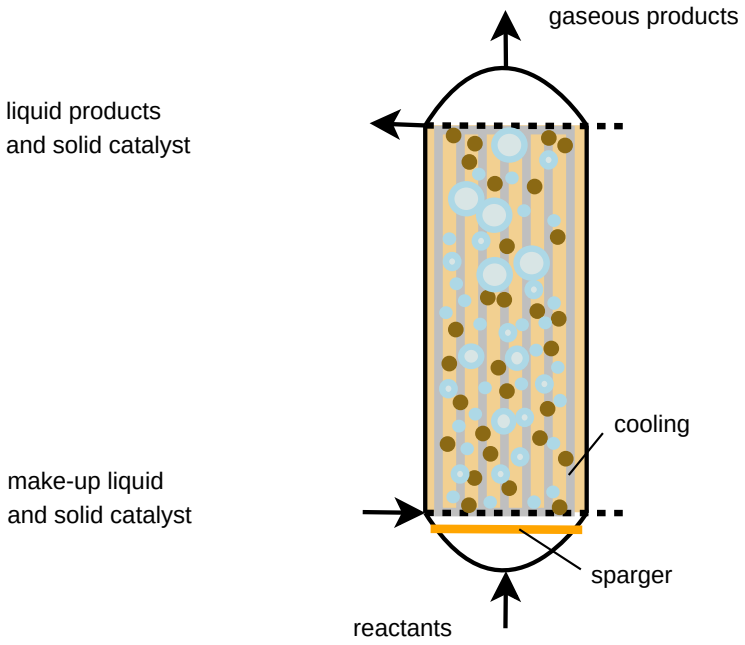

Figure 1: Slurry bubble column (Vik et al., 2015).

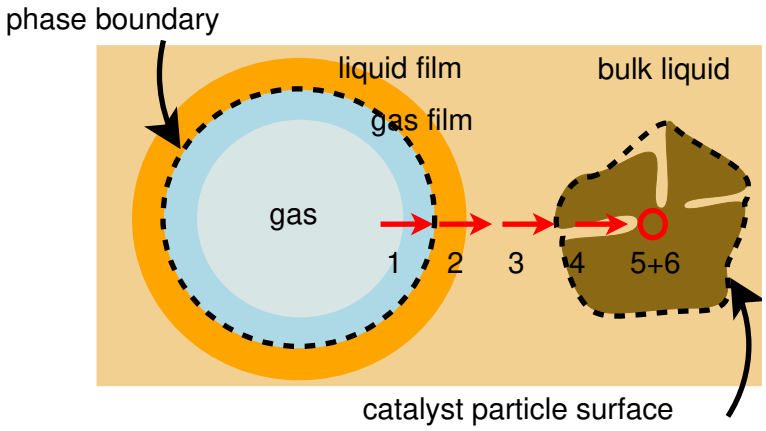

Figure 2: Resistances observed by the reactants on their way to become products in the FTS in a slurry bubble column (Vik et al., 2015). The liquid film resistance (2), is the most important.

Table 1: Physical properties, reactor dimensions and operating conditions for the FTS at industrial conditions (LTFT) with a high loading of cobalt catalyst.[1] Sehabiague and Morsi (2013a), [2] Maretto and Krishna (2001), [3] Sehabiague (2012), [4] Sehabiague et al. (2008), [5] Sehabiague and Morsi (2013b)(Table 3 for Heavy F-T Cut at 530 K), [6] Post et al. (1989), [7] Yates and Satterfield (1991), [8] Maretto and Krishna (1999), [9] Erkey et al. (1990).

parameter		**value**	**reference**
Reactor height	H	15 m	chosen
Reactor inner diameter	D_C	3 m	chosen
Reactor hydraulic diameter	D_H	0.4 m	calc.
Distance between cooling tubes	D_t	114 mm	[1]
Temperature	T	513 K	[2]
Pressure	p	3 MPa	[2]
Bubble size range	ξ	0.1 – 25 mm	chosen
Inlet bubble Sauter-mean diameter (SMD)	d_s	5-15 mm	[3]
Gas volume fraction	α_G	0.5 m^3/m^3	chosen
Gas density (average)	ρ_G	10 kg/m^3	calc.
Gas superficial velocity	v_z^s	0.26 m/s	[4]
Gas–liquid surface tension	σ_{G-L}	0.016 N/m	[5]
Liquid volume fraction	α_L^0	0.28 m^3/m^3	chosen
Liquid density	ρ_L	687.2 kg/m^3	[5]
Liquid viscosity	μ_L	0.6 mPa s	[6]
Liquid superficial velocity	v_L^s	0.01 m/s	chosen
Solid volume fraction	α_S	0.22 m^3/m^3	chosen
Volume fraction catalyst in gas-free slurry	ϕ_S	0.44 kg/kg	chosen
Solids skeleton density	ρ_S	3154 kg cat/m^3 cat	[7]
Solids average particle diameter	d_S	72 μm	[7]
Solid superficial velocity	v_S^s	8×10^{-3} m/s	chosen
Slurry density	ρ_{SL}	1800 kg/m^3	calc.
Slurry viscosity	μ_{Sl}	0.7 mPa s	calc.
H_2/CO ratio, inlet	n_{H_2}/n_{CO}	2 kmol/kmol	chosen
Weight fraction CO_2, inlet	ω_{CO_2}	0.1 kg/kg	chosen
Turbulent dissipation rate	ϵ	2.55 m^2/s^3	$\epsilon = u_G^0 g$
Product distribution parameter	α	0.9	[8]
Diffusion coefficients	D_s		[9]
Henry's law coefficients	K_s		Appendix D

Table 2: Factors found in the literature to influence the gas-liquid mass transfer coefficient k_L. + indicates that an increase in the factor gives an increase in the k_L value and −− indicates that an increase in the factor gives a decrease in the k_L value. The number of signs indicate the magnitude of the effect, as evaluated by the authors of this work. * Increase in column diameter leads to more liquid turbulence, which increases k_L Han et al. (2011). For small columns Yang et al. (2001) found k_L to decrease with column width.

factor	**effect on k_L**	**reference**
increase in contact time τ	–	e.g. Higbie (1935)
increase in internal circulation in the bubble	+	
increase in relative velocity u_r	++	Higbie (1935)
*	at the interface	
increase in contamination or surface agents	–	Calderbank and Moo-Young (1961)
increase in surface mobility	+	Higbie (1935)/ Frössling (1938) Calderbank and Moo-Young (1961)
deviation from spherical shape	complex	Olsen et al. (2017)
increase in liquid (continuous phase) viscosity	–	Yang et al. (2001)
addition of solid particles	–	Yang et al. (2001), Beenackers and Van Swaaij (1993)
increase in pressure	–	Shaikh and Al-Dahhan (2013), Fukuma et al. (1987) , Rollbusch et al. (2015)
increase in temperature	++	e.g. Yang et al. (2001)
increase in dispersion height	–	Calderbank and Moo-Young (1961)
increase in column diameter	++ / –	*
bubble swarm compared to single bubble	-	Hughmark (1967a)
increase in liquid turbulence	++	Han et al. (2011)

Table 3: Selected correlations for the liquid side mass transfer coefficient.

author	correlation	validity range	system
Higbie (1935)	$k_L = 2\sqrt{\frac{D}{\pi\tau_e}}$, $\tau_e = \frac{\xi}{v_t}$	slightly soluble gases	single bubbles in liquid; 3 mm ID test tube. CO_2 in water
Frössling (1938)	$Sh = 2 + 0.6Re_p^{1/2}Sc^{1/3}$, $Sh = \frac{k_L\xi}{D}$, $Re_p = \frac{u_r\xi}{\nu_G}$, $Sc = \frac{\nu_L}{D}$	$0.2 < \xi < 1.8$ mm $0.2 < u_G < 7$ m/s	Nitrobenzene, aniline and water droplets in air
Hughmark (1967a)	$Sh = 2 + 0.0187 \times \left[Re_p^{0.494}Sc^{0.339}\left(\frac{\xi g^{1/3}}{D^{2/3}}\right)^{0.072}\right]^{1.61}$, $Re_p = \frac{u_s\xi}{\nu_L}$	Tested for $500 < Re^{0.494}Sc^{0.339}\left(\frac{\xi g^{1/3}}{D^{2/3}}\right)^{0.072} < 1500$	bubble swarm in a BC
Hughmark (1967b)	$Sh = A + BRe_p^m Sc^n$	Single "solid spheres" in liquid; $1 < Re_p < 10000$	single sphere
Brauer (1981)	$Sh = 2 + 0.015Re_p^{0.89}Sc^{0.70}$, $Re_p = \frac{u_\infty\xi}{\nu_L}$	turbulent mass transfer to non-spherical bubbles with stochastic deformations of the interface $10^5 < Sc < 10^8$	single bubble in turbulent liquid
Akita and Yoshida (1974)	$Sh = 0.5Sc^{1/2}Ga^{1/4}Bo^{3/8}$, $Sh = \frac{k_L d_{vs}}{D}$, $Ga = \frac{gd_{vs}^3}{\nu_L^2}$, $Bo = \frac{gd_{vs}^2\rho_L}{\sigma}$	$Bo < 400$ $D_c < 0.6$ m $\epsilon_G < 0.3$ $u_G^s < 0.42$ m/s not suitable for rapid absorption $480 < Sc < 1600$	bubbles in liquid; square BC, sides 0.077 m and 0.15 m
Fukuma et al. (1987)	$Sh = 4.5 \times 10^{-4}Sc^{0.5}Ga^{0.8}Bo^{-0.2}$	$3.2 \times 10^5 < Ga < 2.6 \times 10^8$ $1.4 < Bo < 120$	bubbles in slurry; SBC, ID 0.15 m
Fortescue and Pearson (1967)	$k_L = 1.46\sqrt{\frac{D\sqrt{2}\epsilon^{1/3}}{L^{2/3}}}$	$800 < Re < 3000$ (laminar), $3000 < Re < 10000$ (turbulent)	bubbles in liquid; channel flow through grid
Lamont and Scott (1970)	$k_L = 0.4\left(\frac{\nu_L}{D}\right)^{-1/2}(\epsilon\nu)^{1/4}$	$5000 < Re < 15000$, predicts within a factor of 2	bubbles in turbulent pipe flow
Han et al. (2011)	$\overline{k_\lambda} = \frac{2}{\pi}\sqrt{\frac{2DA}{L}}\int_0^{\pi/2}\sqrt{cos(\phi)}\mathrm{d}\phi$ $k_L = \frac{\int_\kappa \overline{k_\lambda}E(\kappa)\mathrm{d}\kappa}{\int_\kappa E(\kappa)\mathrm{d}\kappa}$ $E(\kappa) = C\epsilon^{2/3}\kappa^{-5/3}\times \left(\frac{\kappa\lambda_e}{[(\kappa\lambda_e)^2+c_L]^{1/2}}\right)^{5/3+p_0}\times \exp\left(-\beta\left[(n\eta)^4 + c_\eta^4\right]^{1/4} + \beta c_\eta\right)$	$2 \times 10^{-4} < \epsilon < 0.5$	bubbles in turbulent liquid; BC and stirred tank
Yang et al. (2001)	For H_2: $Sh = 1.546 \times 10^2 Eu^{0.052}Re^{0.076}Sc^{-0.231}$ For CO: $Sh = 8.748 \times 10^2 Eu^{-0.012}Re^{0.024}Sc^{-0.133}$ $Eu = \frac{P}{\rho_{SL}(u_G^s)^2}$, $Re = \frac{u_G^s D_c}{\nu_{SL}}$, $Sc = \frac{\nu_{SL}}{D}$, $Sh = \frac{k_L D_c}{D}$	$3.6 \times 10^6 < Eu < 1.5 \times 10^8$ $8 < Re < 340$ $13 < Sc < 270$ $293 < T < 523$ K 1 MPa $< p < 5$ MPa $0.05 < \phi_S < 0.2$ $0.002 < u_G^s < 0.02$	bubbles in slurry; SBC, ID 0.037 m
Calderbank and Moo-Young (1961)	For "small bubbles", $\xi < 2.5$mm: $k_L = 0.31Sc^{-2/3}\left(\frac{\Delta\rho\mu_c g}{\rho_c^2}\right)^{1/3}$ $Sc = \frac{\mu_c}{\rho_c D}$ For "large bubbles", $\xi > 2.5$mm: $k_L = 0.42Sc^{-1/2}\left(\frac{\Delta\rho_L\mu_c g}{\rho_c^2}\right)^{1/3}$	$0.2 < \xi < 8$ mm $0.7 < \rho_L < 1.2$ kg/m^3 $0.6 < \mu_l < 87$ m Pa·s	bubbles in liquid, droplets in air, solid particles in liquid. CO and H_2 in wax amongst other

Table 4: List of simulations. The first column indicates the k_L value for CO, the second column the source of the value. The third column is the inlet SMD. The first set of six simulations varied the k_L model but kept the SMD and all other process conditions (Table 1) constant. The second set of four simulations were run with different inlet SMD. The final three simulations varied the slope of k_L (slope given in the first column) with the same mean value of $k_L = 0.4$ mm/s (see also Figure 6).

$\mathbf{k_{L,CO}}$ mm s^{-1}	**source**	$\mathbf{d_{s,in}}$ mm
0.2	Deckwer et al. (1980)	10
0.5-1	Higbie (1935)	10
0.8-1.4	Akita and Yoshida (1974)	10
1.5	Han et al. (2011)	10
0.4	Calderbank and Moo-Young (1961)	10
3	Vandu and Krishna (2004)	10
0.4	Calderbank and Moo-Young (1961)	5
0.4	Calderbank and Moo-Young (1961)	8
0.4	Calderbank and Moo-Young (1961)	15
0.4	Calderbank and Moo-Young (1961)	20
0.4	model 1	10
$0.2 + 0.026.7\xi$	model 2	10
$0.6 - 0.026.7\xi$	model 3	10

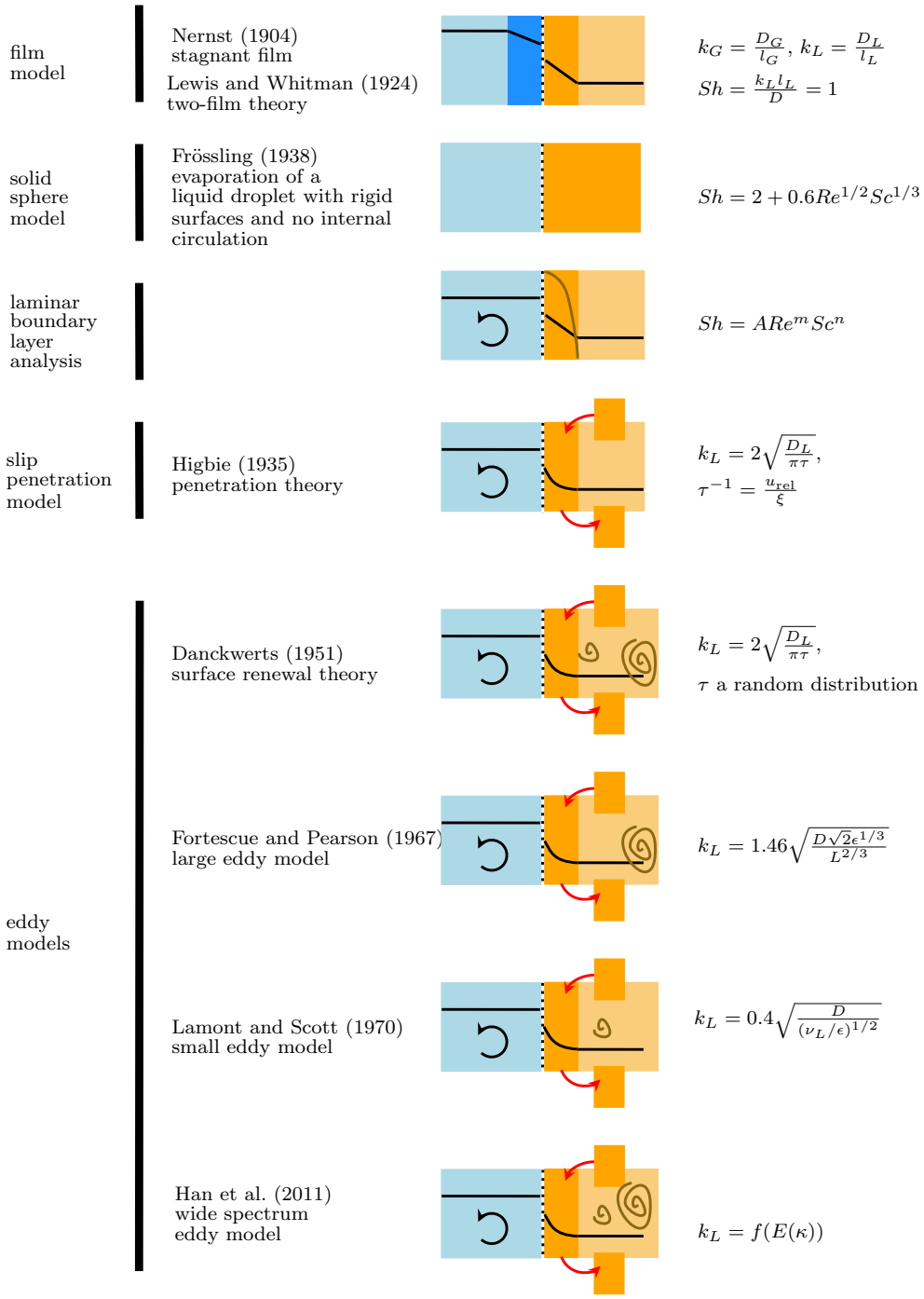

Figure 3: Simplified illustration of the main differences between gas-liquid mass transfer theories. Blue area indicates gas, the light orange area indicates liquid. The light blue area is the bulk gas phase, the dark blue area is the gas layer closest to the interface. The light orange are is the bulk liquid phase, the dark orange area is the liquid layer closest to the interface. The dashed line represents the interface. The solid line illustrates concentration.

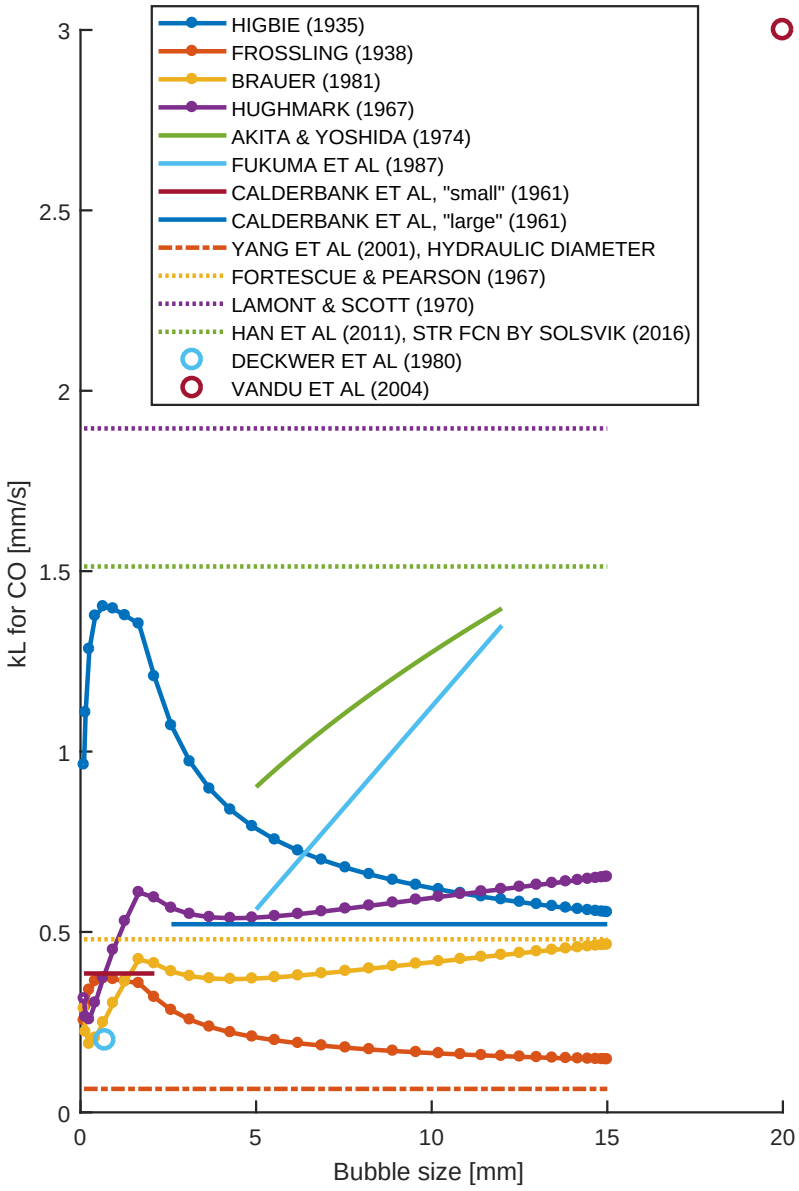

Figure 4: The gas-liquid mass transfer correlations in Table 3 and the experimental values by Deckwer et al. (1980) and Vandu and Krishna (2004) as functions of bubble size for the conditions specified in Table 1. Note that the correlations by Akita and Yoshida (1974) and Fukuma et al. (1987) depend on the SMD.

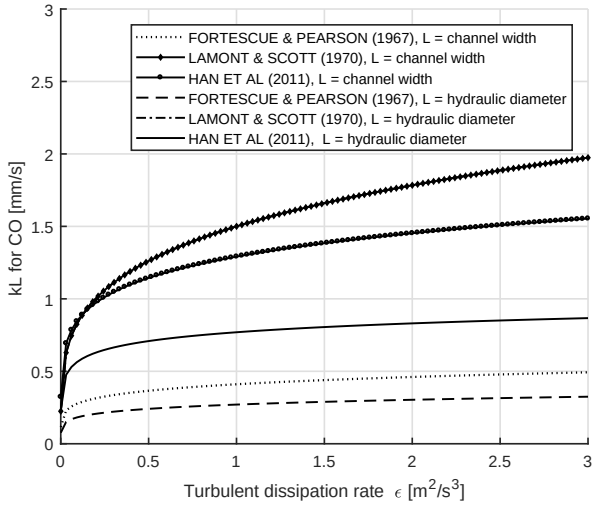

Figure 5: Gas-liquid mass transfer coefficients based on turbulence theory with two choices of length scales as the largest (integral) scale; distance between two cooling rods $D_t = 0.114$ m (applied in this work) and hydraulic diameter of the column $D_{c,h} = 0.45$ m. The correlation by Lamont and Scott (1970) does not depend on the length scale and thus the curves for this correlation overlap with each other.

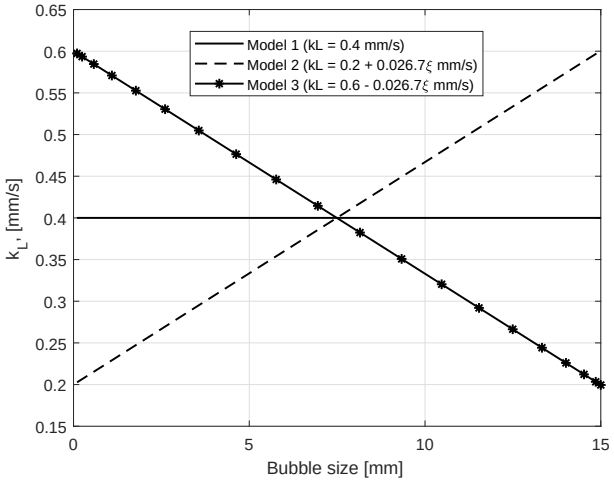

Figure 6: Gas-liquid mass transfer coefficient values as function of bubble size for the constructed models 1, 2 and 3. Model 1 corresponds to the value by Calderbank and Moo-Young (1961) and is constant for all ξ. Model 2 increases linearly throughout the domain, model 3 decreases. Model 2 and 3 have equal slopes with opposite sign and equal means. The mean of model 2 and the mean of model 3 are both equal to the value of model 1.

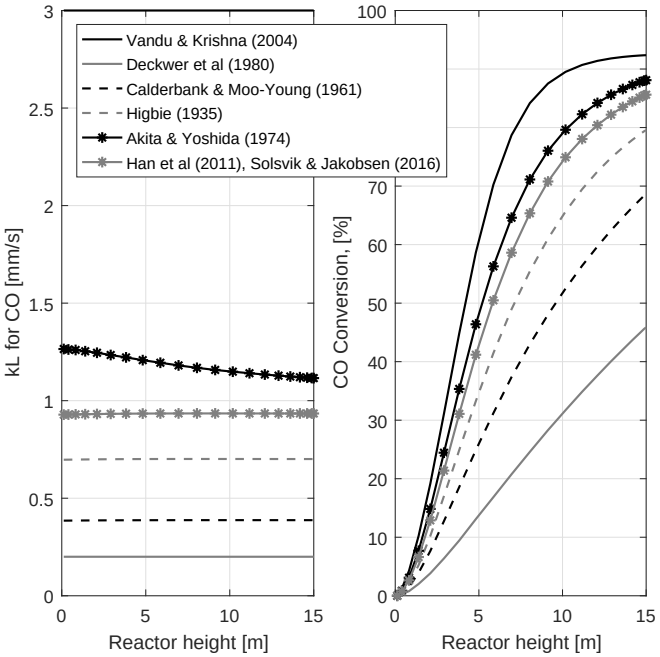

Figure 7: Gas-liquid mass transfer coefficient and resultant conversion of CO.

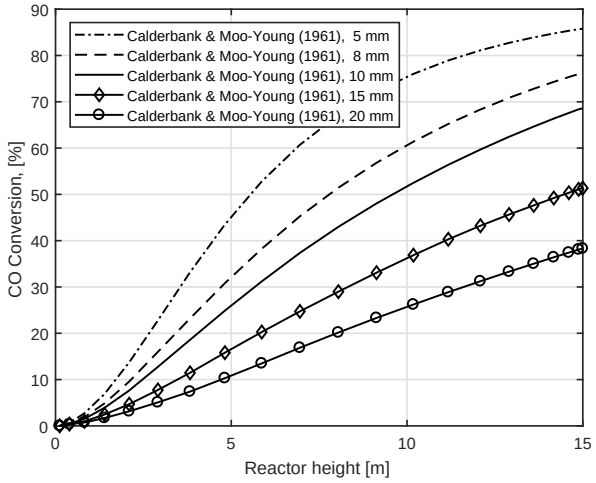

Figure 8: Conversion as a function of reactor length for inlet SMD 5, 8, 10, 15 and 20 mm. k_L value from (Calderbank and Moo-Young, 1961).

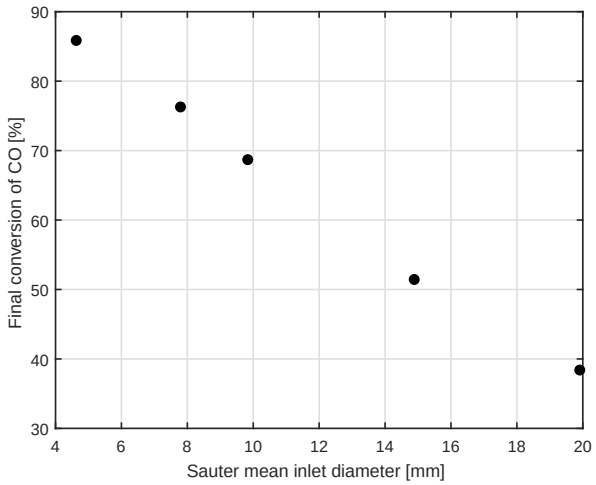

Figure 9: Final conversion as a function of inlet SMD. k_L value from (Calderbank and Moo-Young, 1961).

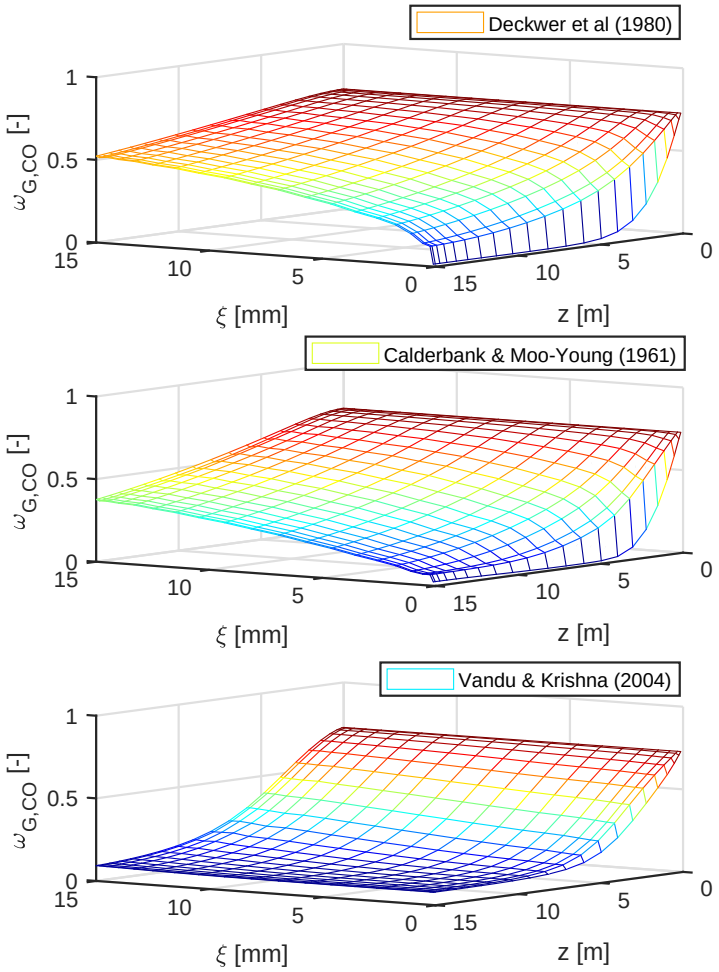

Figure 10: Weight fraction of CO k_L values 0.2 mm/s (Deckwer (1992), upper plot), 0.4 mm/s (Calderbank and Moo-Young (1961), middle plot) and 3 mm/s (Vandu and Krishna (2004), lower plot).

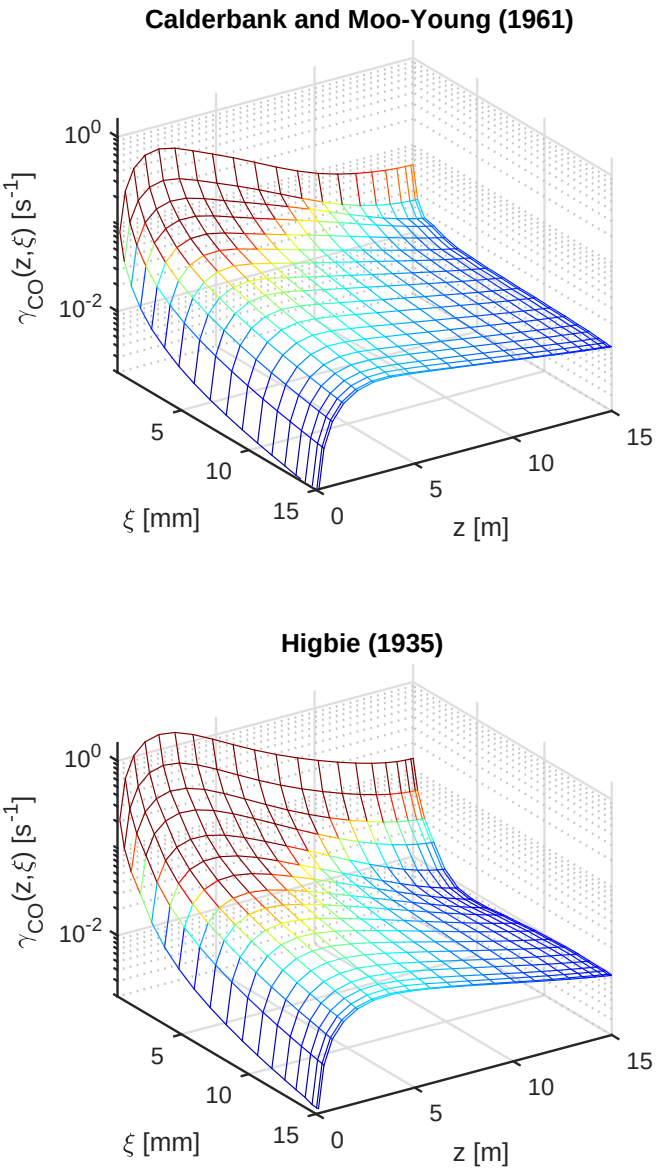

Figure 11: $\gamma_s(z,\xi)$ as a function of axial direction and bubble size for two different k_L correlations; Calderbank and Moo-Young (1961) and Higbie (1935).

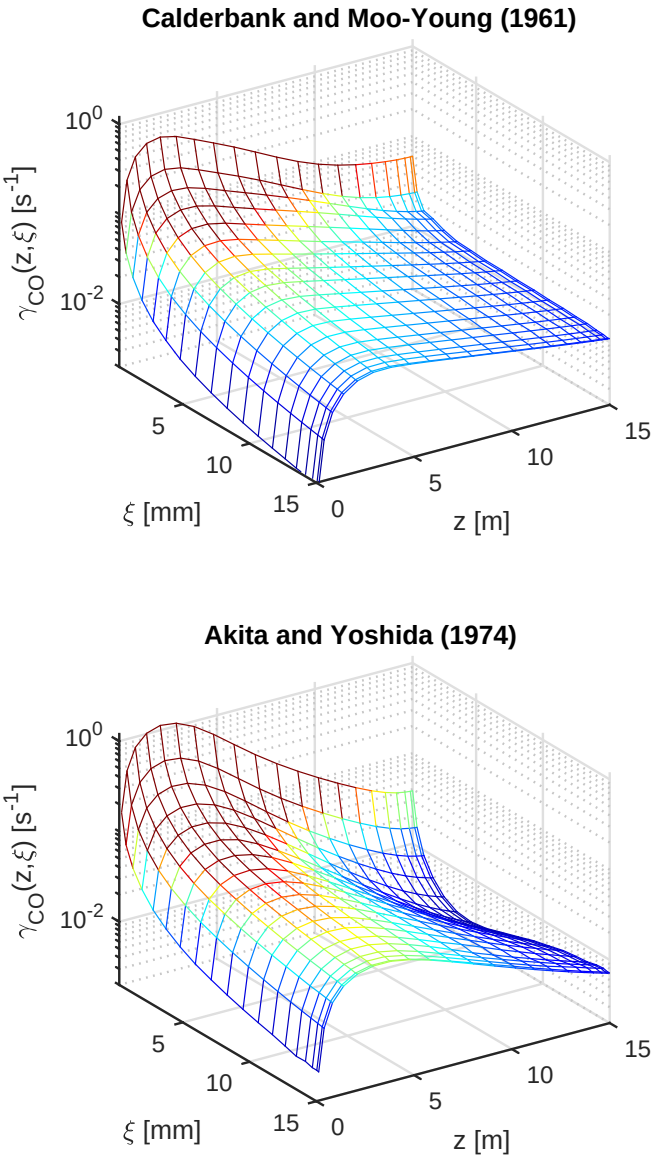

Figure 12: $\gamma_s(z,\xi)$ as a function of axial direction and bubble size for two different k_L correlations; Calderbank and Moo-Young (1961) and Akita and Yoshida (1974).

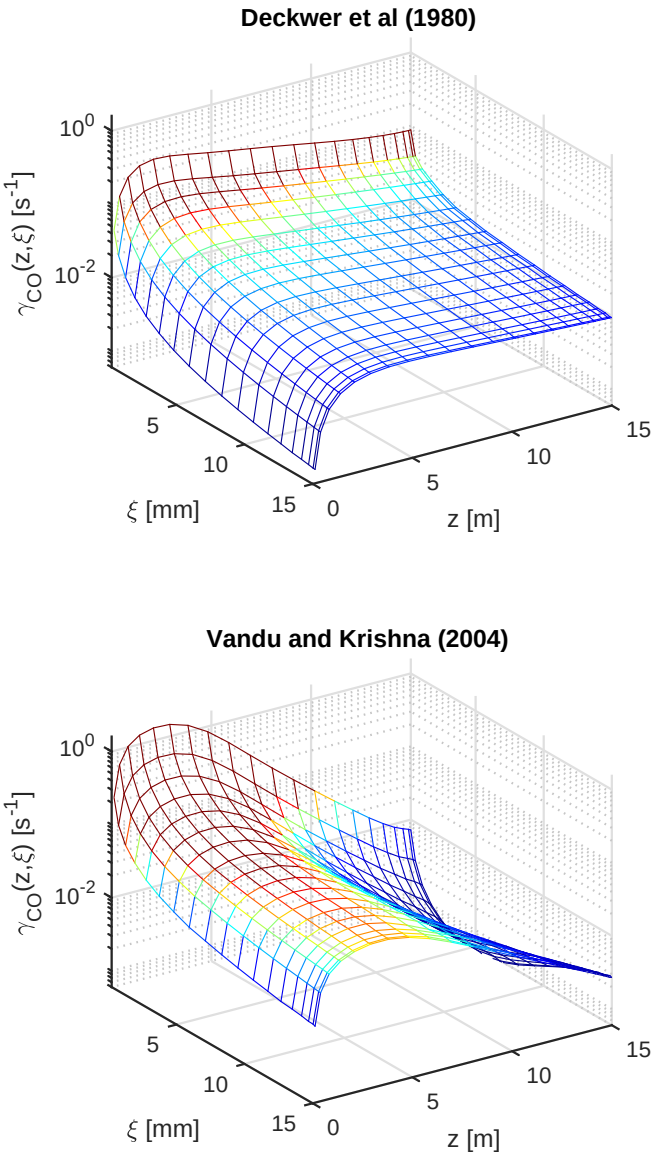

Figure 13: $\gamma_s(z,\xi)$ as a function of axial direction and bubble size for two different k_L correlations; Deckwer et al. (1980) and Vandu and Krishna (2004).

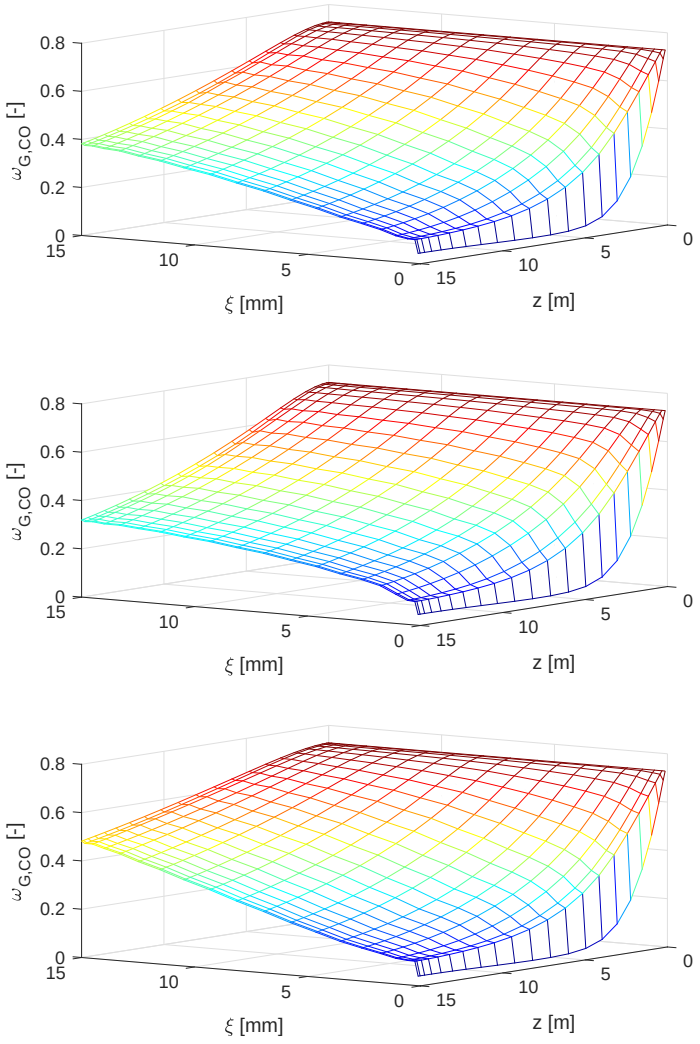

Figure 14: Resultant weight fraction of reactant as a function of axial direction and bubble size for the illustrative models 1, 2 and 3 (see Figure 6 and Table 4).

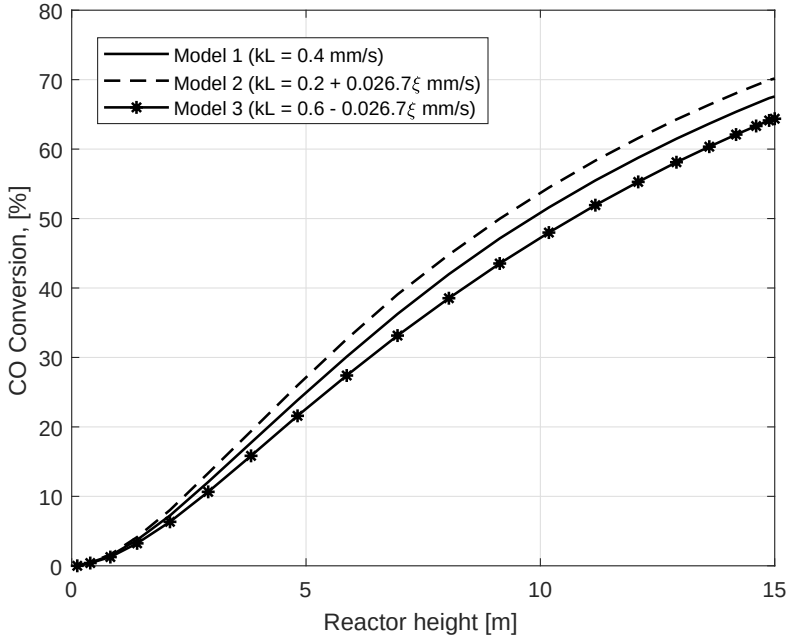

Figure 15: Conversion as a function of axial direction for the illustrative models 1, 2 and 3 (see Figure 6 and Table 4).

Appendix A. Additional relations

Appendix A.1. Calculation of effective dispersion and conduction coefficients

The effective (and turbulent) gas dispersion coefficient was found with basis in the relationship between the turbulent viscosities in the gas and liquid phases presented by (Grienberger, 1992), page 104:

$$\mu_{t,G} = \mu_{t,L} \frac{\rho_G}{\rho_L} R_p^2 \tag{A.1}$$

where the factor R_p was the relationship between the turbulent fluctuations in the phases, given as:

$$R_p = \sqrt{\frac{\overline{(u_i' u_j')_G}}{(u_i' u_j')_L}} \tag{A.2}$$

As the relationship in Eq. (A.2) was not possible to determine in a precise way experimentally, R_p was instead estimated by the ratio of the velocity fluctuations in the axial direction;

$$R_p = \sqrt{\frac{\overline{(u_z' u_z')_G}}{(u_z' u_z')_L}} \tag{A.3}$$

R_p was then found experimentally to be in the order of magnitude 1 (Grienberger, 1992), page 54. Thus one may simplify Eq. (A.1) to saying that the kinematic viscosity is equal in gas and liquid phases:

$$\nu_G = \nu_L \rightarrow \frac{\mu_G}{\rho_G} = \frac{\mu_L}{\rho_L} \rightarrow \mu_G = \mu_L \frac{\rho_G}{\rho_L} \tag{A.4}$$

We may thus write for the effective (and turbulent) gas dispersion coefficient:

$$D_{G,z,\text{eff}} = \frac{\rho_G}{\rho_L} D_{L,z,\text{eff}} \tag{A.5}$$

The effective liquid dispersion coefficient $D_{L,z,\text{eff}}$ was found from the relation by Deckwer et al. (1974) (re-written into SI units):

$$D_{L,z,\text{eff}} = 0.68 D_c^{n_D} (v_{G,\text{in}}^s)^{0.3} \tag{A.6}$$

where $n_D = 1.4$. n_D is corrected using the expression by Yang and Fan (2003):

$$n'_D = n_D \left(1 - 0.11 \ln\left(\frac{\rho_G}{\rho_{G,0}}\right)\right) \tag{A.7}$$

where $\rho_{G,0}$ is the density of the gas at ambient pressure and temperature. This gives for the conditions in this model $n'_D = 0.960$ which gives a liquid dispersion coefficient of $D_{L,z,\text{eff}} = 3.741[\text{m}^2/\text{s}]$. The Reynolds analogy was applied to calculate the effective turbulent viscosity for the gas and liquid phases as follows:

$$\begin{aligned} \mu_{L,z,\text{eff}}(z) &= D_{L,z,\text{eff}} \rho_L(z) \\ \mu_{G,z,\text{eff}}(z,\xi) &= D_{G,z,\text{eff}} \rho_G(z,\xi) \end{aligned} \tag{A.8}$$

whilst for the solid phase $\mu_{S,z,\text{eff}} = 1$ as for granular flow (constant particle viscosity, CPV model (Jakobsen, 2014), page 1406. The Reynolds analogy was applied to calculate the effective turbulent thermal conductivities for the gas and slurry phases were calculated using:

$$\lambda_{G,z,\text{eff}} = D_{G,z,\text{eff}} \rho_G C_{p,G} \tag{A.9}$$

$$\lambda_{L,z,\text{eff}} = D_{L,z,\text{eff}} \rho_L C_{p,L} \tag{A.10}$$

Appendix A.2. Continuous phase equations of change for species mass

The equation of change for liquid species mass is given as:

$$\frac{\partial}{\partial z}\left(v_L(z) \rho_L \omega_{L,s}(z)\right) = -\frac{d j_{L,s}(z)}{dz} + \Gamma_s(z) + R_s(z) \tag{A.11}$$

$$j_{L,s}(z) = -\rho_L D_{L,z,\text{eff}}(z) \frac{d\omega_{L,s}(z)}{dz} \tag{A.12}$$

with boundary conditions:

$$\begin{aligned} j_{L,s}(z)|_{z=H} &= 0 \\ \omega_{L,s}(z)|_{z=0} &= \omega_{L,s,\text{in}} \end{aligned} \tag{A.13}$$

and where the mass transfer term is given as:

$$\Gamma_s(z) = \int_{\xi_{\min}}^{\xi_{\max}} f_d(z,\xi)\gamma_s(z,\xi)\mathrm{d}\xi \tag{A.14}$$

Appendix B. The impact of solids on breakage, coalescence and bubble terminal velocity

The slurry bubble column in this work has a very high solids loading (44 vol%) and thus a note on the effects of such a large solids fraction on the bubble breakup, bubble coalescence and terminal velocity is in place.

The collision between a particle of the same order of magnitude as the bubble may lead to particle penetration into the bubble and subsequent bubble breakup (Chen and Fan 1989). A high solids fraction increases the probability of bubble breakup given a penetration event (Chen and Fan, 1989). However, in this work the particles are of size 72 μm whilst the bubbles are in the range 0.1-25 mm and thus penetration is not likely to occur. As bubble breakup is a result of collision between bubbles and turbulent eddies (Prince and Blanch, 1990) the effect a high solids fraction has on the turbulence also affects bubble breakup. So whilst large particles may increase bubble breakage, Sarhan et al. (2018) suggested that the increase in solid concentration of small particles ($\sim$100 μm) decreased the bubble breakup rate because the presence of solid particles dampened the liquid turbulence. A lower gas-liquid surface tension increases bubble breakage (Chilekar et al., 2010).

The effect of solid particles on coalescence is governed by different mechanisms. At the micro level, addition of solid particles appears to increase the coalescence time

and thus reduce coalescence (Ata, 2008) with the result of a net reduction of the Sauter-mean diameter with increasing solid concentration (Sarhan et al., 2016). The particle lyophility is of importance (Chilekar et al., 2010). A lyophilic solid particle in an SBC experiences strong forces of attraction between the solid particle and the liquid and will thus be present in the liquid phase. On the contrary, a lyophobic particle will have strong forces of repulsion between the particle and the liquid and will be more likely to adhere to the gas-liquid surface of a bubble. It can thus be a coalescence inhibitor as it prevents film drainage. A lyophilic particle will be present in the liquid and have less effect on film drainage, as shown in Figure B.1. In contrast to the foregoing points, the majority of studies report that the Sauter-mean diameter in general decreases with increasing solids concentration (e.g. de Swart et al. (1996); Ojima et al. (2014, 2015); Sarhan et al. (2018); Tyagi and Buwa (2017)). It must be noted that coalescence and breakage are competing phenomena. To determine single breakage and coalescence events experimentally for high solids density flows is challenging, thus the reported increased gas holdups or decreased Sauter-mean diameters mean that breakage has increased in favor of coalescence.

Bubble size, surface tension (through the Eötvös number in the drag coefficient), the level of turbulence and solid particle adhesion impact the terminal velocity of the bubbles (Evans et al. (2008); Ojima et al. (2014); Tomiyama (1998), respectively). Larger bubbles have higher terminal velocity than smaller (e.g. Ojima et al. (2014)). The bubbles tend to travel longer paths and thus have a reduced terminal velocity in turbulent conditions (Evans et al., 2008). Solid particles adhered to the bubbles slow the bubble down due to reduced buoyancy (Evans et al., 2008).

Whether or not the solid particles adhere to the bubbles depends on the surface chemistry of the solid particles, the chemistry of the solution and its surfactants and the surface forces (Xing et al., 2017). In a particle-attachment process, a particle collides with a bubble, slides around it whilst thinning the liquid film between the particle and the bubble, forms a three-phase contact and eventually attaches (Xing et al., 2017). A number of forces, such as gravity and hydrodynamic forces, may detach the solid particle from the bubble. In particular, the turbulent energy dissi-

pation rate and turbulent eddies are found to play a role. Also, the surface features of the solid particle play an important role in the detachment (Xing et al., 2017).

As discussed by Chilekar et al. (2010), whether or not the particles adhere to the gas-liquid (bubble) interface depends on the particles being lyophilic or lyophobic. The applied catalyst material is alumina (as carrier) with cobalt (or iron), the liquid phase consists of paraffins and the gaseous phase consists of water, some CO, CO2, H2 and hydrocarbons. As alumina is polar, it is likely to have a larger affinity towards the gaseous phase than the liquid phase, as hydrocarbons are nonpolar. Based on this, it is probable that the particles may to some extent adhere to the gas-liquid interface, thus being present in the liquid film outside the bubbles. This topic may also be related to the contamination of bubbles discussed by e.g. Calderbank and Moo-Young (1961), which increases as the column height increases (as the bubbles have more time in contact with the contaminants in the liquid). However, a more detailed knowledge on the surface forces acting between the solid, liquid and the gas phases at the simulated conditions are required to conclude on the issue of particle-bubble attachment.

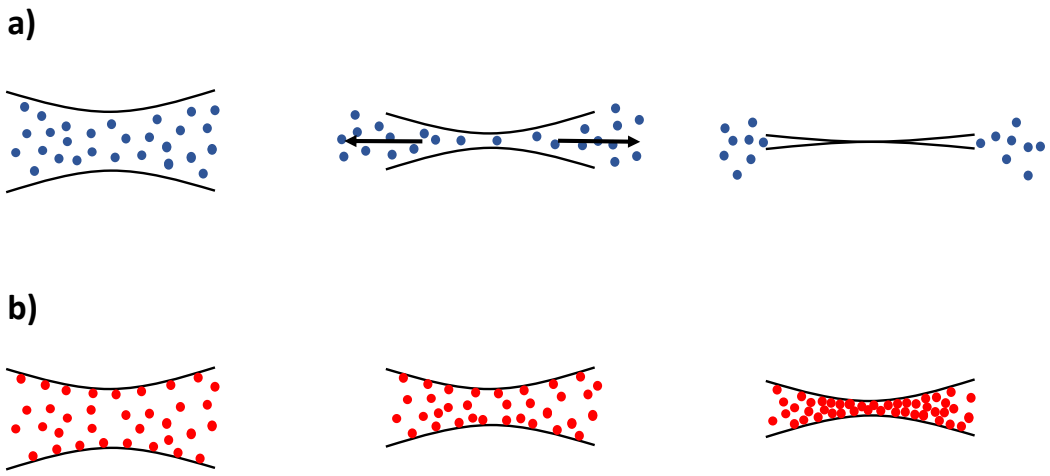

Figure B.1: An illustration of the coalescence event for (a) lyophilic particles and (b) lyophobic particles, adapted from Chilekar et al. (2010). Lyophilic particles decrease the film thinning time as they contribute to the thinning of the film by dragging the liquid out with them. Lyophobic particles, in contrast, are stuck at the gas-liquid interface and thus represent a steric barrier which increases the film thinning time and thus reduces coalescence.

Appendix C. Dimensionless numbers

Table C.1: Dimensionless numbers.

dimensionless number	**expression**	**reference to application**	**value for the conditions in Table 1**
Reynolds number	$Re = \frac{v_L D_H}{\nu_L}$	Lamont and Scott (1970)	1.09×10^4
Reynolds number	$Re = \frac{v_G^s D_C}{\nu_{SL}}$	Yang et al. (2001)	2.8×10^6
Reynolds number	$Re = \frac{v_{G,t}\xi}{\nu_L}$	Brauer (1981)	$(0.0006 - 4.7) \times 10^3$
Reynolds number	$Re = \frac{4Q}{\nu_L w}$	Fortescue and Pearson (1967), where Q is the total flow rate and w is the wetted perimeter	1.2×10^5
Integral scale Reynolds number	$Re_L = \sqrt{\frac{kL}{\nu_L}} = \frac{k^2}{\epsilon \nu_L}$	Solsvik and Jakobsen (2016)	8.7×10^4
Taylor scale Reynolds number	$Re_\lambda = \sqrt{\frac{20}{3} Re_L}$	Solsvik and Jakobsen (2016)	759
Particle Reynolds number	$Re_p = \frac{v_G^s \xi}{\nu_L}$	Hughmark (1967a), Hughmark (1967b), Brauer (1981)	$(0.03{-}4.5){\times}10^3$
Particle Reynolds number	$Re_p = \frac{v_r \xi}{\nu_G}$	Frössling (1938)	NA
Schmidt number	$Sc = \frac{\nu}{D}$	Frössling (1938), Hughmark (1967a), Hughmark (1967b), Brauer (1981), Fukuma et al. (1987), Akita and Yoshida (1974)	67
Sherwood number	$Sh = \frac{k_L d_s}{D}$	Akita and Yoshida (1974), Fukuma et al. (1987)	$(3.8 - 38) \times 10^5 k_L$
Sherwood number	$Sh = \frac{k_L \xi}{D}$	Frössling (1938), Hughmark (1967a), Hughmark (1967b), Brauer (1981)	$(0.076 - 38) \times 10^5 k_L$
Sherwood number	$Sh = \frac{k_L D_c}{D}$	Yang et al. (2001)	$6.8 \times 10^8 k_L$
Galilei number	$Ga = \frac{g d_s^3}{\nu_L^2}$	Akita and Yoshida (1974), Fukuma et al. (1987)	6.6×10^6
Eötvös or Bond number	$E\ddot{o} = Bo = \frac{\Delta \rho g d_s^2}{\sigma}$	Akita and Yoshida (1974), Fukuma et al. (1987)	25
Euler number	$Eu = \frac{p}{\rho_{SL} u_G^2}$	Yang et al. (2001)	5.9×10^5

Appendix D. Values for the Henry's law coefficients

The Henry's law coefficients applied in Eq. (3) were calculated using by use of Aspen HYSYS for the simulated process conditions. Their values are given in Table D.1 below.

Table D.1: Calculated values for the Henry's law coefficients applied in Eq. (3).

component	**value**
CO	310
H_2	390
H_2O	144
CO_2	158
C_1	210
C_2	116
C_3	72.8
C_4	45.5
C_5-C_{12}	9.12
C_{13}-C_{22}	10.8
C_{23}-C_{30}	8.68
C_{31+}	0.0686